UNRAVELING CRP/cAMP-MEDIATED METABOLIC REGULATION IN *ESCHERICHIA COLI* PERSISTER CELLS

Han G. Ngo[1], Sayed Golam Mohiuddin[1], Aina Ananda[2], Mehmet A. Orman[1,*]
[1]Department of Chemical and Biomolecular Engineering, University of Houston, TX, 77204
[2]Department of Biology, Monmouth University, NJ, 07764
[*]Corresponding author: morman@central.uh.edu

ABSTRACT

A substantial gap persists in our comprehension of how bacterial metabolism undergoes rewiring during the transition to a persistent state. Also, it remains unclear which metabolic mechanisms become indispensable for persister cell survival. To address these questions, we directed our efforts towards persister cells in *Escherichia coli* that emerge during the late stationary phase. These cells have been recognized for their exceptional resilience and are commonly believed to be in a dormant state. Our results indicate that the global metabolic regulator Crp/cAMP redirects the metabolism of these antibiotic-tolerant cells from anabolism to oxidative phosphorylation. Although our data demonstrates that persisters exhibit a reduced metabolic rate compared to rapidly growing exponential-phase cells, their survival still relies on energy metabolism. Extensive genomic-level analyses of metabolomics, proteomics, and single-gene deletions consistently highlight the critical role of energy metabolism, specifically the tricarboxylic acid (TCA) cycle, electron transport chain (ETC), and ATP synthase, in sustaining persister levels within cell populations. Altogether, this study provides much-needed clarification regarding the role of energy metabolism in antibiotic tolerance and highlights the importance of using a multipronged approach at the genomic level to obtain a broader picture of the metabolic state of persister cells.

INTRODUCTION

Bacterial persisters within cell cultures constitute a small subpopulation of cells exhibiting a transient antibiotic-tolerant state (Balaban et al., 2004). While persisters have traditionally been characterized as non-growing and dormant phenotypes (Lewis, 2010), recent studies challenge these conventional hallmarks, revealing the heterogeneity of persister cells in terms of growth, metabolism, and other cellular activities (Adams et al., 2011; Arnoldini et al., 2014; Hossain et al., 2023; Ma et al., 2010; Mok, Park, et al., 2015; Orman & Brynildsen, 2013a, 2015; Shan et al., 2015; Wakamoto et al., 2013). Despite potential discrepancies in research outcomes in the field, we think that these variations arise from the intricate and diverse survival mechanisms employed by bacterial cells in response to adverse conditions, such as antibiotic treatments. Furthermore, the interplay of stochastic and deterministic factors associated with these mechanisms adds another layer of complexity, with outcomes highly contingent on factors such as cell types, antibiotics, and experimental and growth conditions (Michiels et al., 2016). The persistence phenomenon presents a significant health concern (Huemer et al., 2020; Murray et al., 2022), as the transient antibiotic-tolerant state of persister cells promotes recurrent infections (Fisher et al., 2017) and establishes them as a reservoir for the emergence

of antibiotic-resistant mutants (Barrett et al., 2019; Levin-Reisman et al., 2017; Windels et al., 2019).

Drug tolerance is a widespread phenomenon observed in both prokaryotic and eukaryotic cell types. Otto Warburg's research in the early twentieth century unveiled an intriguing aspect of mammalian cell metabolism known as "aerobic glycolysis," wherein proliferating cells (e.g., tumor cells) derive energy predominantly through glycolysis, even in the presence of oxygen (Warburg, 1925). This metabolic reprogramming involves restricting entry into the TCA cycle through precise enzymatic control, diverting glycolytic intermediates towards anabolic pathways. This adaptation supports the extensive biosynthesis required for active cell proliferation in tumors (Hanahan & Weinberg, 2011). Remarkably, tumorigenic persisters that exist in a non-proliferating state may not primarily depend on aerobic glycolysis. Instead, there is substantial evidence suggesting that these cells rely on energy metabolism (Porporato et al., 2018; Vasan et al., 2020); however, the presence of this metabolic state in antibiotic-tolerant bacteria is still a question mark (Orman & Brynildsen, 2015). Reprogramming energy metabolism seems to be an evolutionarily conserved strategy for cells facing stress or adverse conditions, as these cells might benefit from the significantly higher ATP production efficiency provided by oxidative phosphorylation (Hanahan & Weinberg, 2011). The identification of a mechanism shared by diverse cell types could open avenues for the development of global strategies to target drug-tolerant cells effectively.

A recent study suggests that bacterial persisters constitute a stochastically formed subpopulation of low-energy cells, despite some observed overlap in ATP levels between antibiotic-sensitive and persister cells (Manuse et al., 2021). The persister cells examined in that study were derived from an aged stationary phase culture (48 hours post-inoculation) (Manuse et al., 2021), a condition known to elevate the number of non-growing cells, which do not promptly resume growth upon transfer to a fresh medium (Mohiuddin, Kavousi, et al., 2020). While the non-growing cells formed during the stationary phase have reduced metabolic activity compared to growing cells, as demonstrated in our earlier study (Orman & Brynildsen, 2013a), they still exhibit a certain degree of respiratory activity (Orman & Brynildsen, 2015). In a recent study measuring ATP levels in viable but non-culturable (VBNC; a phenotype that is antibiotic tolerant but unable to resume growth after antibiotic removal), persister and antibiotic-sensitive cells from 24-hour stationary phase cultures, a significant overlap in intracellular ATP concentrations was observed between antibiotic-sensitive and persisters cells (Li et al., 2024). On the other hand, VBNC cells exhibited drastically lower ATP levels compared to both persister and antibiotic-sensitive cells (Li et al., 2024). Another independent study, which utilized single-cell analysis, reported that ofloxacin persisters were metabolically active cells in exponentially growing cultures before treatment and these cultures were obtained from 16-hour overnight precultures (not aged) (Goormaghtigh & Van Melderen, 2019). These findings suggest that while persisters formed during exponential growth may initially retain metabolic activity, they may gradually transition to reduced energy states as they age within the culture. The nature of persister-cell metabolism in bacteria is a topic that has long been a point of contention in scientific circles. The controversy surrounding this topic primarily arises from studies that rely on bacteriostatic chemicals or a limited number of gene deletions, or direct comparisons to exponentially growing cells, all of which have inherent drawbacks

(Conlon et al., 2016; Manuse et al., 2021; Orman & Brynildsen, 2013a, 2015). The metabolism of persister cells, a very complex phenomenon, cannot be easily characterized by a simplistic term such as "metabolic dormancy". Even if persister cells may exhibit a lower metabolism compared to the vast majority of rapidly growing exponential-phase cells, they may still rely on energy metabolism for their functioning (Amato et al., 2014; Prax & Bertram, 2014). In fact, analyzing published studies collectively suggests that bacterial cell metabolism undergoes intricate alterations or rewiring as they transition into a tolerant state, and these alterations seem to be highly dependent on the specific conditions tested (Adams et al., 2011; Arnoldini et al., 2014; Ma et al., 2010; Mok, Park, et al., 2015; Orman & Brynildsen, 2013a, 2015; Shan et al., 2015; Wakamoto et al., 2013).

To gain a better understanding of the critical role of energy metabolism in persister cell survival, we have focused our research on antibiotic-tolerant cells formed during the stationary phase, given that these cells are known to be highly resilient and capable of surviving a variety of stressors, including antibiotics, and are assumed to be dormant (Balaban et al., 2004; Orman & Brynildsen, 2015). These cells are also referred to as type I persisters, which cannot readily resume growth when diluted in fresh media during the lag phase (Balaban et al., 2004). Previous studies showed that these persister cells can metabolize specific carbon sources that make them susceptible to aminoglycosides (AG) (Allison et al., 2011; Mok, Orman, et al., 2015; Orman & Brynildsen, 2013b). Their AG susceptibility is due to increased AG uptake, which is facilitated by increased ETC activity and membrane potential (Allison et al., 2011). The presence of active energy metabolism in antibiotic-tolerant, non-growing cells may indeed explain their rapid killing by AG in the presence of carbon sources (Orman & Brynildsen, 2013b, 2015). When the knockout strains of global transcriptional regulators (i.e., ArcA, Cra, Crp, DksA, Fnr, Lrp, and RpoS) were screened using the AG potentiation assay in our previous study, the results showed that the panel of carbon sources tested potentiated the AG killing of tolerant cells derived from most knockout strains, except for Δ*crp* and Δ*cyaA* (Mok, Orman, et al., 2015). This can be attributed to the lack of active energy metabolism in these mutant strains, as the Crp/cAMP potentially shapes persister cell metabolism during the stationary phase. Depletion of primary carbon sources activates adenylate cyclase (CyaA) (Pastan & Perlman, 1970), increasing cyclic-AMP (cAMP) levels in cells (Bettenbrock et al., 2007; Park et al., 2006). The cAMP molecules, along with its receptor protein (Crp), activate genes related to the catabolism of secondary carbon sources, potentially supporting cellular functions and energy levels (Deutscher, 2008; Fic et al., 2009; Görke & Stülke, 2008; Kolb et al., 1993). Here, using metabolomics, proteomics, and high-throughput screening of single-gene deletion strains, we have provided evidence that the Crp/cAMP regulatory complex maintains an active state of energy metabolism while downregulating anabolic pathways in the antibiotic-tolerant persister cells.

RESULTS

Disruption of the Crp/cAMP complex affects the formation of persister cells at the late stationary phase.

Since Crp/cAMP-mediated metabolic changes can be induced by nutrient depletion during the stationary phase, we wanted to assess the effects of deleting the *crp* and *cyaA* genes (Δ*crp* and

127 Δ*cyaA*) on both persister cell formation and metabolism during this phase. As anticipated, the
128 deletion of the *cyaA* gene resulted in a notable reduction in intracellular cAMP concentration
129 (**Figure 1—figure supplement 1**). However, the Δ*crp* strain exhibited an increase in cAMP
130 concentration, potentially due to the negative feedback regulatory mechanism of the
131 Crp/cAMP complex for the *cyaA* gene promoter (Keseler, 2004; Majerfeld et al., 1981) (**Figure**
132 **1—figure supplement 2**). When comparing the growth curves of *E. coli* wild-type (WT), Δ*crp*,
133 and Δ*cyaA* main cultures under identical conditions studied here (see **Materials and Methods**),
134 all three strains started to enter the stationary phase around 5 hours, with the mutant strains
135 exhibiting slightly lower optical density levels than the WT at this time point (**Figure 1—figure**
136 **supplement 3**). Also, our data provide evidence of an increase in cAMP levels in WT cells during
137 their transition into the stationary phase (**Figure 1—figure supplement 4**), aligning with existing
138 literature (Bettenbrock et al., 2007; Keseler, 2004; Park et al., 2006). For type I persister
139 quantification, we diluted cells in the fresh medium, consistent with previous studies (Balaban
140 et al., 2004; Orman & Brynildsen, 2015), at early (t=5 h) and late (t=24 h) stationary phases and
141 subsequently exposed them to an extended period (20 h) of ampicillin or ofloxacin treatment
142 (200 µg/mL ampicillin and 5 µg/mL ofloxacin). These treatments were carried out at
143 concentrations surpassing the minimum inhibitory concentrations (MIC), necessary for the
144 selection of antibiotic-tolerant persister cells (**Supplementary File 1**) (Keren, Kaldalu, et al.,
145 2004). Also, type I persisters, formed during the stationary phase, exhibit a slow transition from
146 a non-growing state to an active state when transferred to a fresh medium in the lag phase
147 (Balaban et al., 2004; Jõers & Tenson, 2016; Orman & Brynildsen, 2015; Vulin et al., 2018);
148 therefore, this transition requires longer antibiotic treatment durations. Moreover, we
149 transferred an equal number of cells from each strain to the fresh medium to ensure
150 consistency in cell numbers. To assess persistence, we collected samples during antibiotic
151 treatment, washed them to remove antibiotics, and plated them on agar media to quantify
152 colony-forming units (CFU) of surviving cells (see **Materials and Methods**). The resulting
153 biphasic kill curves—plots of CFU levels over treatment time—are characteristic of persistence
154 phenotypes (**Figure 1**). Notably, the WT strain showed a marked increase in both ampicillin- and
155 ofloxacin-persister cells during the late stationary phase, in contrast to the mutant strains,
156 where no such increase was observed (**Figure 1A, B**). However, this trend was not observed in
157 the early stationary phase (**Figure 1A, B**). To confirm that the observed decrease in persister
158 levels in the mutant strains in the late stationary phase is solely attributed to the perturbation
159 of the Crp/cAMP regulatory network, we reintroduced *crp* expression to the Δ*crp* strain using a
160 low-copy plasmid carrying the *crp* gene and its promoter. As a control, we utilized an empty
161 vector of the same plasmid. The results demonstrated that the expression of *crp* restored the
162 persister level in the mutant strain, while the plasmid itself had no impact on persister levels
163 (**Figure 1—figure supplement 5A, B**). Altogether, these findings highlight the significant role of
164 Crp/cAMP in ampicillin and ofloxacin persister formation in the late stationary phase.

165 Ampicillin and ofloxacin, both broad-spectrum antibiotics with a strong dependence on cell
166 metabolism (E. J. Zheng et al., 2020), target cell wall synthesis and DNA gyrase activity,
167 respectively. In addition to these two antibiotics, we also quantified aminoglycoside-persister
168 levels in both WT and mutant strains. This was achieved by exposing diluted cells from both
169 early and late stationary phases to 50 µg/mL gentamicin, a concentration exceeding the MIC

levels (**Supplementary File 1**). After prolonged gentamicin exposure (20 h), the tolerant cell colonies were found to be below the limit of detection for all strains and conditions (**Figure 1C, and Figure 1—figure supplement 5C**). Although bacterial tolerance can vary significantly depending on the specific antibiotics and growth phase used (Hofsteenge et al., 2013), this outcome contrasts starkly with the observed levels of ampicillin and ofloxacin persisters in WT (**Figure 1**). The mechanism by which aminoglycosides eliminate persister cells in the WT strain may be linked to their metabolism, given that aminoglycoside uptake is an energy-requiring process (Allison et al., 2011; Taber et al., 1987), and this aspect will be explored further in the subsequent section.

We would like to highlight that antibiotic concentrations, washing procedures (to remove antibiotics), and agar plate incubation times for CFU enumeration may affect experimental outcomes. However, variations in these parameters, including lower antibiotic concentrations normalized to the MIC of each strain (5× or 10× MIC; see **Figure 1—figure supplement 6**), additional washing steps to ensure complete removal of antibiotics (see **Figure 1—figure supplement 6**), and extended agar plate incubation times of up to 48 hours (see **Figure 1—figure supplement 7**), did not affect the persistence phenotype. The Δ*crp* and Δ*cyaA* strains consistently showed reduced ampicillin and ofloxacin persistence compared to WT, whereas all three strains showed no detectable persisters following gentamicin treatment (**Figure 1—figure supplement 6, 7**). Moreover, we examined the impact of Crp/cAMP disruption in the HipA7 strain to assess whether the role of Crp/cAMP in persistence extends to a genetically sensitized, persister-enriched background. Deletion of either *crp* or *cyaA* in the HipA7 background significantly reduced persistence to both ampicillin and ofloxacin during the late stationary phase (**Figure 1—figure supplement 8**), mirroring the effects observed in the WT strain. Altogether, these results show that disruption of the Crp/cAMP regulatory network impairs persister formation during the late stationary phase, underscoring its critical role in ampicillin and ofloxacin tolerance.

Crp/cAMP complex governs *E. coli* stationary phase metabolism.

To determine whether the reduced ampicillin and ofloxacin persister levels at the late stationary phase in the mutant strains (**Figure 1A, B**) are linked to stationary phase metabolism, we utilized untargeted mass spectrometry (MS). This approach facilitated the quantification of metabolites in Δ*crp* cells, allowing for a comparison with WT controls in both the early and late stationary phases (**Figure 2A**). Since both Δ*crp* and Δ*cyaA* strains exhibit the same persistence phenotype, and *crp* deletion effectively abolishes Crp/cAMP complex function, we used the Δ*crp* mutant for metabolomic profiling to capture key regulatory changes while maintaining experimental feasibility. The metabolomics data were subjected to unsupervised hierarchical clustering, and metabolites identified in independent biological replicates of each strain and condition were found to cluster together (**Figure 2A**), thus confirming the reproducibility of our data.

To elucidate the upregulated and downregulated metabolic pathways in the mutant strain as compared to the WT strain, we performed enrichment analyses utilizing MetaboAnalyst (Lu et al., 2023). For downregulated pathways, we considered a threshold ratio of 0.5 or lower, where the ratio indicates metabolite levels in the mutant strain relative to the WT (**Supplementary**

212 **File 2A**). Conversely, for upregulated pathways, the threshold ratio was set at 2 or higher
213 (**Supplementary File 2B**). The enrichment ratio for each pathway was calculated based on the
214 number of metabolite hits compared to the expected hits derived from the chemical structure
215 library (Lu et al., 2023). Our extensive comparison of the mutant cells to the WT cells through
216 pathway enrichment analysis (refer to **Figure 2B** and **Figure 2—figure supplement 1-3** for
217 pairwise comparison of different conditions) revealed several important findings:

218 **(i)** During the early stationary phase, we observe a slight downregulation in the abundance of
219 TCA cycle metabolites, including citrate and fumarate, in the Δ*crp* strain compared to WT
220 (**Figure 2C** and **Figure 2—figure supplement 1**). However, as the late stationary phase
221 progresses, the downregulation in both TCA cycle and pentose phosphate metabolism becomes
222 more pronounced in the Δ*crp* strain (**Figure 2B, D**).
223 **(ii)** The Δ*crp* strain exhibits upregulation of several metabolites compared to WT during both
224 early and late stationary phases, primarily associated with anabolic pathways. Particularly, the
225 upregulation of some of these pathways becomes more pronounced during the late stationary
226 phase. These pathways include crucial metabolites like deoxyribonucleosides and
227 ribonucleosides (which play essential roles in DNA and RNA synthesis), fatty acids and
228 carboxylic acids (the main components of bacterial cell membranes), and peptides (which are
229 linked to protein synthesis) (**Figure 2B**).
230 **(iii)** During the early stationary phase, we noticed a significant upregulation in the abundance of
231 intermediate metabolites related to glycolysis, gluconeogenesis, and pyruvate metabolism in
232 mutant cells compared to WT cells (**Figure 2C**). This observation is not surprising, as the
233 inhibition of the TCA cycle in the mutant strain could potentially redirect metabolic fluxes
234 toward glycolysis and lactate metabolism.

235 Altogether, our metabolic data indicate that, in the stationary phase, WT cells maintain their
236 energy metabolism to some extent while downregulating their anabolic pathways (**Figure 2A**).
237 This metabolic state appears to be regulated by the Crp/cAMP complex, as perturbing its
238 function leads to a significant downregulation of energy metabolism and an upregulation in the
239 abundance of anabolic metabolites (**Figure 2B**).

240 **Proteomics analysis revealed upregulated pathways in the Δ*crp* strain associated with**
241 **anabolic metabolism, alongside the downregulation of key proteins in energy metabolism.**

242 Since the Crp/cAMP complex acts as a transcriptional regulator affecting the expression of
243 metabolic proteins whose abundance directly affects cellular metabolites, we performed
244 untargeted proteomics, our second genomic-level study, to further validate our results.
245 Considering the noticeable metabolic alterations observed during the late stationary phase, we
246 utilized MS to quantify proteins in Δ*crp* cells and compared them to WT controls at this stage.
247 The resulting proteomics data were subjected to unsupervised hierarchical clustering, and the
248 proteins identified in independent biological replicates of each strain were found to cluster
249 together, confirming the consistency of our findings (**Figure 3—figure supplement 1**). By
250 analyzing protein-protein association networks and employing functional enrichment through
251 STRING (Szklarczyk et al., 2021, 2023), which integrates various functional pathway
252 classification frameworks such as Gene Ontology annotations, KEGG pathways, and UniProt
253 keywords, we pinpointed various upregulated and downregulated pathways in the mutant

254 strain when compared to the WT (**Supplementary File 3**). The upregulated pathways are
255 associated with anabolic metabolism and encompass peptidoglycan metabolic processes, cell
256 wall organization or biogenesis, cellular component organization or biogenesis, regulation of
257 cell shape, cell cycle, and cell division (**Figure 3A**). Also, the mutant strain displayed
258 downregulated pathways, encompassing glycerol metabolism, TCA cycle, pyruvate metabolism,
259 glycolysis, and various pathways associated with ribosome and transcriptional factor activity
260 (**Figure 3B)**. Our analysis specifically pinpointed a cluster of proteins involved in energy
261 metabolism and respiratory processes. Notably, this cluster includes GltA, SdhB, SucC, SucD,
262 FrdB, FrdA, AcnA, AceA, and Mdh proteins, which play crucial roles in either the TCA cycle or as
263 membrane-bound components of ETC (**Figure 3B**). Altogether, the alignment between
264 metabolomics and proteomics analyses provides additional validation for the Crp/cAMP-
265 mediated metabolic state.

266 **Crp/cAMP complex shapes *E. coli* cell proliferation dynamics.**

267 The omics data suggest that the upregulation in the abundance of anabolic metabolites and
268 proteins, particularly those related to cell wall organization or biogenesis, cell cycle, and cell
269 division, in the stationary-phase mutant cells, would likely enhance their ability to resume
270 growth upon transitioning to fresh medium. To investigate this, we utilized a cell proliferation
271 assay that employed an inducible fluorescent protein (mCherry) expression cassette. This assay
272 provided us with the ability to monitor non-growing cells at a single-cell resolution, as described
273 previously (Orman & Brynildsen, 2013a; Roostalu et al., 2008). The mCherry expression cassette
274 is controlled by an isopropyl ß-D-1-thiogalactopyranoside (IPTG) inducible synthetic T5
275 promoter that was previously inserted into the chromosome of an *E. coli* strain carrying a *lacI*^{q}
276 promoter mutation (Orman & Brynildsen, 2013a). This configuration allowed for precise
277 regulation of mCherry expression using IPTG. Here, we introduced *crp* and *cyaA* deletions into
278 this strain. These deletions reduced the persistence of the mCherry-expressing *E. coli* strain in
279 the late stationary phase (**Figure 4—figure supplement 1**), consistent with the findings
280 presented in **Figure 1**. To perform the growth assay, we induced mCherry expression in the
281 main cultures and then washed the cells to remove IPTG. The cells were then inoculated into a
282 fresh medium without IPTG and their growth was analyzed with a flow cytometer. This allowed
283 us to track the dilution of mCherry protein within the cells, which served as an indicator of cell
284 proliferation. As shown in **Figure 4A**, initially, all cells exhibited high red fluorescence. However,
285 as cells underwent division, the red fluorescence of the overall population decreased in the
286 absence of the inducer (**Figure 4A**). Notably, within the WT strain, a subpopulation from the
287 late stationary phase cultures displayed constant fluorescence levels, indicating their inability to
288 divide (**Figure 4B**). In contrast to the WT strain, we did not detect similar subpopulations in the
289 mutant strains (**Figure 4B**). Additionally, this subpopulation of non-growing cells does not
290 emerge during the early stationary phase cultures (**Figure 4A**). This observation provides an
291 explanation for the observed reduction in persister levels in these mutant strains in the late
292 stationary phase, as the enrichment of persister cells within these non-growing cell
293 subpopulations was reported in previous studies (Joers et al., 2010; Orman & Brynildsen,
294 2013b; Roostalu et al., 2008).

295 To confirm the significance of Crp/cAMP in the formation of non-growing cells, we introduced
296 the expression plasmid carrying the *crp* gene into the Δ*crp* strain. As anticipated, the

297 introduction of the *crp* expression plasmid resulted in the emergence of a non-growing
298 population within the culture, contrasting with the mutant strain containing the empty plasmid
299 vector used as a control (**Figure 4—figure supplement 2A, B**). The reduced capacity of
300 stationary-phase WT cells to initiate proliferation upon transfer to a fresh medium suggests the
301 possible presence of an extended lag phase in these cells. To investigate this, we employed flow
302 cytometry to precisely quantify cell numbers and generate growth curves for both WT and
303 mutant strains. As anticipated, the growth curve of the WT strain displayed a slower initial
304 growth rate and a prolonged lag phase duration compared to the mutant strains (**Figure 4C**).
305 Conversely, the mutant strains displayed a shorter lag phase, yet they demonstrated an
306 increased doubling time in the exponential phase compared to WT (**Figure 4C**), which was also
307 anticipated, considering their decreased reliance on oxidative phosphorylation due to TCA cycle
308 inhibition. Altogether, these results provide additional support and validation for the findings
309 from our metabolomics and proteomics data, as our data reveals a correlation between the
310 abundance of molecules associated with cell division and the ability of the stationary phase
311 cells to resume growth.

312 **Persister cells rely on energy metabolism.**

313 The Crp/cAMP-mediated metabolic state, characterized by increased respiration in WT
314 compared to mutant strains, was further validated using redox sensor green (RSG) dye and a
315 reporter plasmid measuring the promoter activity of succinate:quinone oxidoreductase (SQR)
316 genes. The SQR reporter system (Zaslaver et al., 2006) employs green fluorescent protein (GFP)
317 expression, regulated by the promoter of the SQR operon, which includes the *sdhA*, *sdhB*, *sdhC*,
318 and *sdhD* subunit genes. The SQR complex plays a vital role in cellular metabolism by catalyzing
319 the oxidation of succinate to fumarate concurrently with the reduction of ubiquinone to
320 ubiquinol, thus directly linking the TCA cycle with the respiratory ETC (Keseler, 2004). Our
321 results indicate an upregulation of the SQR promoter activity in WT cells compared to the
322 mutant strains in the stationary phase, validating the findings from our metabolomics and
323 proteomics data (**Figure 5A**). The RSG dye, on the other hand, serves as a well-established
324 metabolic indicator, measuring bacterial oxidation-reduction activity, a crucial function
325 involving the ETC driven by the TCA cycle. Once reduced by bacterial reductases, the RSG dye
326 emits a stable green fluorescent signal (**Figure 5—figure supplement 1**). Our data demonstrate
327 that the redox activities of WT cells are much higher and more heterogeneous compared to
328 those of the mutant strains in the late stationary phase, further corroborating the results from
329 our preceding analyses (**Figure 5B**). Furthermore, we utilized a methodology that integrates the
330 mCherry expression system, flow cytometry, and ampicillin-mediated cell lysis, to determine
331 whether persister cells in WT still maintain their respiration. In this assay, both the WT and
332 mutant strains carrying the mCherry expression system were exposed to ampicillin after
333 transferring them to a fresh medium. The inducer was added to both growth and treatment
334 cultures to sustain the cells' red signals. Unlike other antibiotics, ampicillin disrupts cell wall
335 synthesis, leading to the lysis of cells upon their resumption of growth. As seen in **Figure 5—**
336 **figure supplement 2**, the cells that were lysed lost their mCherry signals. On the other hand,
337 the resilient, tolerant cells that evaded ampicillin-induced lysis maintained their mCherry levels
338 throughout the treatment. In the mutant strains, ampicillin was effective in lysing almost all
339 cells as anticipated, leaving no or small number of intact cells (**Figure 5—figure supplement 2**).

However, in the WT strain, we detected a subpopulation of intact cells throughout the entire treatment period (**Figure 5C,** and **Figure 5—figure supplement 2**). While the population-level redox activities of these tolerant intact cells in WT are lower than those of exponential phase cells, they still displayed a significant increase in RSG levels compared to cell populations before antibiotic treatments or untreated control cells subjected to identical conditions (**Figure 5D**), suggesting that they maintain steady-state energy metabolism. We want to highlight that not all intact cells in the WT strain reported here are persisters. A significant portion comprises 'viable but non-culturable' (VBNC) cells, and WT cells exhibit markedly higher VBNC levels than Δ*crp* and Δ*cyaA* strains (**Figure 5—figure supplement 3**). VBNC cells can be quantified from intact cells following beta-lactam treatments (Orman & Brynildsen, 2013b; Roostalu et al., 2008). These cells may exhibit metabolic activities but are unable to readily colonize upon transfer to fresh medium (Ayrapetyan et al., 2018; Orman & Brynildsen, 2013b). Collectively, our metabolic measurement data (**Figure 5A-C**) aligns with the findings from our omics analyses, and the number of intact cells observed in WT after beta-lactam treatment is consistent with the count of non-growing cells in WT (**Figure 4B** vs **Figure 5—figure supplement 2**). These non-growing cells are anticipated to be less susceptible to lysis by beta-lactams (Orman & Brynildsen, 2013b; Roostalu et al., 2008).

The genomic-level screening of *E. coli* knockout underscores the significance of energy metabolism in sustaining the viability of persister cells.

Although some metabolic genes, including those encoding the TCA cycle (e.g., *sdhA, sucB, mdh, icd*), have been studied in *E. coli* (Luidalepp et al., 2011; Ma et al., 2010; Manuse et al., 2021; Orman & Brynildsen, 2015; Yu et al., 2019), a comprehensive genomic-level screening strategy is necessary to validate which metabolic pathways are truly associated with antibiotic tolerance. To further underscore the importance of energy metabolism, we conducted a high-throughput screening of 149 different *E. coli* K-12 BW25113 mutant strains from the Keio knockout library (Baba et al., 2006). The selected strains are related to central carbon metabolism, encompassing glycolysis, pentose phosphate pathways, TCA cycle, ETC, ATP synthase, and fermentation pathways (**Figure 5E**). While the deletion of genes related to glycolysis and pentose phosphate pathways did not affect antibiotic tolerance in the cells, some mutant strains associated with cytochrome bo and quinone oxidoreductase complexes (e.g., *cyo* genes, and *nuoL*) exhibited enhanced tolerance (**Supplementary File 4**). However, the mutant strains exhibited reduced tolerance to both antibiotics compared to the control *E. coli* K-12 BW25113 WT strain were found to be largely associated with the TCA pathway (*sucA, sucB, lpd, sucC, sucD, sdhA, sdhB, sdhC, sdhD, gltA, acnB, aceE, fumA, mdh* and *fumC*), ETC (*nuoB, nuoC, nuoI, nuoK, nuoM,* and *narV*), ATP synthesis (*atpA, atpB, atpC, atpD, atpE,* and *atpH*), and mixed acid fermentation pathways (*ldhA, fdhF, pta, adhE,* and *frdC*) (**Figure 5E,** and **Supplementary File 4**). We acknowledge that the Keio strains were generated in a high-throughput manner, and there might be unknown errors in their genomic DNA. To ensure the reproducibility of our findings, we generated knockout strains for key genes associated with the TCA, ETC, ATP synthase, glycolysis, and pentose phosphate pathway (**Figure 5F**, see **Supplementary File 5** for detailed description of genes). We then tested their antibiotic tolerance, and our results were consistent with the omics data and screening outcomes (**Figure 5F**), confirming the critical role of energy metabolism, specifically the TCA cycle, ETC, and ATP

383 synthase, in bacterial persistence. We note that equal numbers of cells from each strain were
384 transferred into antibiotic treatment media to ensure consistency in cell numbers, and no
385 significant growth deficiencies or differences in cell density were observed in the late stationary
386 phase of the knockout strains (**Figure 5—figure supplement 4**).

387 **DISCUSSION**

388 Our study highlights the crucial role of the Crp/cAMP complex in maintaining the metabolic
389 state of stationary-phase persister cells, enabling their survival under adverse conditions.
390 Through metabolomics, proteomics, and high-throughput screening of single-gene deletion
391 strains, we substantiated that the Crp/cAMP regulatory complex sustains an active respiratory
392 state while downregulating anabolic pathways in persister cells. This respiratory state is vital for
393 the survival of persister cells, as perturbing the Crp/cAMP complex or respiration significantly
394 reduced persister phenotypes, which may explain the previously reported decrease in antibiotic
395 tolerance in *E. coli* cells cultured under anaerobic conditions (Orman & Brynildsen, 2015).
396 Notably, we observed an upregulation of anabolic metabolites and proteins when the
397 Crp/cAMP regulatory complex was perturbed, particularly those associated with cell wall
398 organization, cell cycle, and cell division, enhancing the ability of stationary-phase mutant cells
399 to resume growth. Although the literature has shown associations between antibiotic tolerance
400 with proteins involved in cell division and the TCA cycle (e.g., SdhA, SucB, Mdh) (Luidalepp et
401 al., 2011; Ma et al., 2010; Orman & Brynildsen, 2015; Yu et al., 2019), our study establishes a
402 strong link between these critical cellular processes and the Crp/cAMP complex, providing
403 much-needed clarity in the field. In fact, upon investigating Crp/cAMP regulons via the Ecocyc
404 database (Keseler, 2004), we identified that certain metabolic genes, deleted in our *E. coli* K-12
405 MG1655 background, are potentially regulated by Crp/cAMP (**Supplementary File 5**), providing
406 additional support for the validity of our omics results.

407 We acknowledge that our metabolomic and proteomic data were obtained at the whole-
408 population level, rather than from isolated persister cells. Fluorescent reporters combined with
409 fluorescence-activated cell sorting (FACS) have been utilized to study persister cells, including in
410 our previous studies (Amato et al., 2013; Orman & Brynildsen, 2013a, 2015). However, this
411 approach only enriches for persisters rather than isolating a pure population, as persisters still
412 constitute a small fraction of the sorted cells. Despite these limitations, our population-level
413 analyses provide valuable insights into the role of the Crp/cAMP complex in regulating non-
414 growing cell formation and persistence (**Figure 4**). We further validated these findings through
415 single-gene deletions and flow cytometry-based assays (**Figure 5**), confirming a consistent
416 reduction in both non-growing and persister cells in Crp/cAMP-deficient strains.

417 The deletion of *cyaA* resulted in a reduction of cAMP levels, as expected given the role of the
418 CyaA enzyme in cAMP synthesis (**Figure 1–figure supplement 1**). Conversely, the removal of *crp*
419 led to an increase in cAMP levels compared to those in wild-type cells. Notably, this increase is
420 statistically significant (**Figure 1–figure supplement 1**). Although this is an interesting
421 observation, it is likely due to the feedback regulation of the Crp/cAMP complex on *cyaA*
422 expression (Aiba, 1985; Keseler et al., 2011; Majerfeld et al., 1981). Specifically, disruption of
423 Crp function is expected to derepress the *cyaA* promoter (P_{cyaA}), leading to increased CyaA
424 expression and elevated cAMP levels. To test this, we employed a P_{cyaA}-*gfp* reporter plasmid

425 (pMSs201) in *E. coli* K-12 MG1655 WT, Δ*crp*, and Δ*cyaA* strains to monitor promoter activity. As
426 anticipated, deletion of *crp* led to enhanced *gfp* expression, confirming that Crp/cAMP
427 negatively regulates *cyaA* expression via feedback. These results clarify the observed cAMP
428 differences and support the regulatory role of the Crp/cAMP complex (**Figure 1—figure**
429 **supplement 2**).

430 Our findings reveal substantial heterogeneity in metabolism (measured by RSG) among WT
431 stationary phase cells, contrasting with the more uniform behavior observed in Δ*crp* and Δ*cyaA*
432 strains (**Figure 5B**). We also demonstrated the presence of two distinct populations in WT cells
433 during the late stationary phase: one that resumes rapid growth and another subpopulation
434 that does not resume growth when transferred to a fresh medium (**Figure 4B**). The absence of
435 this non-growing cell subpopulation in the mutant strains could account for their sensitivity to
436 aminoglycosides. However, the mechanism by which aminoglycosides kill these non-growing
437 cells in the WT strain remains perplexing. The underlying reasons might be linked to their
438 metabolism, as aminoglycoside uptake is an energy-requiring process, relying on the electron
439 flow through membrane-bound respiratory chains (Allison et al., 2011). Moreover, persister
440 cells obtained from various antibiotics, such as ampicillin and ofloxacin, in WT *E. coli* were
441 previously found to exhibit sensitivity to aminoglycosides when sugar molecules were
442 introduced into the cultures (Allison et al., 2011; Orman & Brynildsen, 2013b). However, the
443 enhanced sensitivity mediated by sugar molecules was reversed to its original state in a
444 subsequent study when the Crp/cAMP complex was genetically perturbed (Mok, Orman, et al.,
445 2015). This can be attributed to the lack of active energy metabolism in these genetically
446 altered strains, as suggested by our comprehensive genomic-level analyses here. While the
447 absence of cell division in non-growing cell subpopulations in WT may suggest a
448 downregulation in anabolic metabolism, their energy metabolism may remain partially active,
449 which could potentially explain the phenomenon of aminoglycoside potentiation. Indeed, our
450 results presented in **Figure 5D** support this interpretation.

451 Antibiotics are generally effective against proliferating bacteria, leading to the notions that
452 tolerance is linked to temporary growth suppression and that persister cells are dormant
453 phenotypes with repressed metabolism. Although persister cells are generally considered to
454 have reduced metabolic activity compared to exponentially growing cells, their survival may still
455 depend on energy metabolism. Also, the direct comparison of persister cell metabolism to that
456 of exponentially growing cells may not be the best approach. Growing cells have a very high
457 energy output and consume metabolites at a fast pace. Therefore, any comparison between
458 tolerant and non-tolerant cell populations requires proper normalization techniques such as
459 adjusting cellular metabolic activities to the amount of substrate utilized by cells. An example of
460 this normalization was conducted by Heinemann's group (Radzikowski et al., 2016),
461 demonstrating that ATP production rates per substrate in tolerant cells exceed those of
462 exponentially growing cells.

463 We diluted cells in fresh medium at early and late stationary phases before antibiotic
464 treatments. This step is essential for quantifying type I persisters, as these cells do not readily
465 resume growth upon dilution in the fresh medium during the lag phase (Balaban et al., 2004;
466 Orman & Brynildsen, 2015). We acknowledge that antibiotic tolerance is influenced by various
467 factors, including culture dilutions, media, specific strains, antibiotics tested, treatment

468 durations, and the growth phase during treatment administration. These factors may
469 contribute to variations in reported persister levels observed in the Δ*cyaA* strain during the
470 exponential phase (Chu et al., 2012; Molina-Quiroz et al., 2018; Parsons et al., 2024; Sulaiman &
471 Lam, 2020; Yamasaki et al., 2020; A. Zeng et al., 2022). To assess how *cyaA* and *crp* deletions
472 affect antibiotic responses under conditions similar to those used by Zeng et al. (J. Zeng et al.,
473 2022) —specifically, exponential-phase *E. coli* BW25113 strains (Keio collection), lower
474 antibiotic concentrations, and short treatments (e.g., 1 hour)—we first tested *E. coli* MG1655
475 WT, Δ*crp*, and Δ*cyaA* strains in late stationary phase using reduced antibiotic concentrations
476 and shorter exposures. Both knockouts showed decreased survival following ampicillin and
477 ofloxacin treatment compared to WT (**Supplementary File 6**), consistent with our findings in
478 **Figure 1**. In exponential-phase, the knockout strains exhibited reduced survival after ampicillin
479 treatment but increased survival after ofloxacin treatment relative to WT (**Supplementary File**
480 **7A**), again mirroring the trends in **Figure 1**. Gentamicin treatment, however, produced variable
481 results in MG1655 knockouts, likely due to the brief 1-hour exposure being insufficient for
482 robust conclusions (**Supplementary File 7A**). Notably, when we tested the corresponding Keio
483 knockout strains in the BW25113 background, we observed increased tolerance in exponential-
484 phase cells, reproducing Zeng et al.'s findings under their specific conditions (**Supplementary**
485 **File 7B**), although BW25113 and MG1655 exhibited distinct persister phenotypes in exponential
486 phase (**Supplementary File 7A, B**). These results, altogether, highlight the sensitivity of
487 antibiotic tolerance and persistence phenotypes to factors such as strain background, antibiotic
488 concentration, and treatment duration.

489 While we did not focus on the exponential growth phase in our study, it is noteworthy that the
490 reduced growth rate during this phase in the mutant strains (**Figure 4C**) may explain the
491 antibiotic tolerance observed in previous studies involving the *cyaA* deletion (Chu et al., 2012;
492 Molina-Quiroz et al., 2018; Sulaiman & Lam, 2020; Yamasaki et al., 2020). The growth disparity
493 noted between mutant and WT strains, particularly evident around 5 hours in our results
494 (**Figure 1–figure supplement 3**), may also be linked to the ofloxacin persisters observed in the
495 mutant strains at this specific time point (**Figure 1**). While slow cell growth may indeed
496 correlate with bacterial persistence (Kaldalu & Tenson, 2019), it is important to note that the
497 persistence associated with perturbations of metabolic genes cannot be solely attributed to the
498 slow growth. In fact, the persistence of these mutant strains should depend on many factors
499 (see **Supplementary File 5**) as reported by diverse research groups (Kim et al., 2016; Luidalepp
500 et al., 2011; Ma et al., 2010; Orman & Brynildsen, 2015; Pandey et al., 2021; Shan et al., 2015;
501 Spoering et al., 2006; Wang et al., 2018; Yu et al., 2019; Zalis et al., 2019). For instance, in *E.*
502 *coli*, TCA inactivation was shown to decrease ampicillin and ofloxacin persistence during the lag
503 phase (Orman & Brynildsen, 2015), yet it enhances gentamicin tolerance in the exponential
504 phase, which remains unexplained by factors such as cell growth, redox activities, proton
505 motive force (PMF), or ATP levels (Shiraliyev & Orman, 2023). Furthermore, gene deletions
506 often trigger pleiotropic effects, leading to unique tolerance mechanisms not evident in wild-
507 type strains. In our Keio screening data analysis, we observed that the deletion of *icd* appeared
508 to enhance persistence (**Supplementary File 4**), in line with a previous study (Manuse et al.,
509 2021). The *icd* gene encodes a TCA cycle enzyme, isocitrate dehydrogenase. While it remains
510 unclear whether this observed outcome is attributable to other unseen pleiotropic effects

511 stemming from the *icd* deletion, our data consistently indicates that the most significant
512 reduction in persistence levels occurs with disruptions in energy metabolism. A comprehensive
513 approach, encompassing omics and knockout screening as presented in this study, offers a
514 more complete understanding, revealing the consensus behavior within the entire metabolic
515 network.

516 Reactive oxygen species (ROS) have been proposed to contribute to antibiotic killing; however,
517 our prior work using identical experimental conditions demonstrated that ROS are unlikely to
518 be a major factor in persister formation during the late stationary phase (Orman & Brynildsen,
519 2015). In that study, we overexpressed catalytically active antioxidant enzymes, including
520 catalases (KatE, KatG) and superoxide dismutases (SodA, SodB, SodC), yet observed no
521 significant change in persister levels. To further decouple ROS from respiratory activity in that
522 study, we performed anaerobic experiments using nitrate as an alternative terminal electron
523 acceptor. Interestingly, anaerobic respiration enhanced persister formation, and inhibition of
524 nitrate reductases with KCN reduced it—further supporting a ROS-independent mechanism.
525 Together, these findings suggest that under our experimental conditions, it is respiratory
526 activity rather than ROS production that plays a more central role in antibiotic tolerance.

527 In conclusion, a significant gap in the current literature is the lack of a comprehensive
528 understanding of how bacterial cell metabolism undergoes changes during the transition to a
529 tolerant state. Identifying the specific metabolic pathways that gain significance for cell survival
530 in this context is crucial. This knowledge can pave the way for the development of more
531 informed and targeted treatment strategies, ultimately enhancing our ability to combat
532 tolerant cells and improve overall treatment outcomes.

533 **MATERIALS AND METHODS**

534 **Bacterial Strains and Plasmids**

535 All experiments were conducted using *E. coli* K-12 MG1655 wild-type (WT) and its derivative
536 strains. *E. coli* K-12 MG1655, MO strains (carrying the mCherry expression system), *hipA7* (high
537 persister strain) and pUA66 plasmids were obtained from Mark P. Brynildsen at Princeton
538 University. *E. coli* MO strain was used to monitor cell proliferation at single cell level due to its
539 chromosomally integrated isopropyl β-D-1-thiogalactopyranoside (IPTG)-inducible mCherry
540 expression cassette (Orman & Brynildsen, 2013b, 2013a, 2015). *E. coli* K-12 BW25113 WT and
541 single deletions were obtained from Dharmacon Keio Collection (Dharmacon, Catalog#
542 OEC4988, Lafayette, CO, USA). The mutant strains in this study were generated using the
543 Datsenko-Wanner method (Datsenko & Wanner, 2000). The pUA66-EV was generated by the
544 removal of *gfp* gene from the plasmid. The *crp* gene with its promoter was cloned into the
545 modified pUA66 plasmid to obtain the pUA66-*crp* expression system. The *sdhABCD* reporter
546 (pMSs201-$P_{sdhABCD}$-*gfp*) and the *cyaA* reporter (pMSs201-P_{cyaA}-*gfp*) were obtained from a
547 previous study (Zaslaver et al., 2006). The cloning method was followed according to a standard
548 method from NEB (Tirabassi & Bio, 2014). Genetic modifications were verified by PCR and gene
549 sequencing (Genewiz, South Plainfield, NJ, USA). A complete list of strains, plasmids, and
550 oligonucleotides used in this study is presented in the **Key Resources Table**.

551 **Media, Chemicals, and Culture Conditions**

552 All chemicals used in this study were purchased from Fisher Scientific (Atlanta, GA, USA), VWR
553 International (Pittsburgh, PA, USA), or Sigma Aldrich (St. Louis, MO, USA). Luria-Bertani (LB)
554 medium was prepared by combining 5 g of yeast extract, 10 g of tryptone, and 10 g of sodium
555 chloride in 1 L of autoclaved deionized (DI) water. LB agar media was prepared by mixing 40 g of
556 pre-mixed LB agar with 1 L of autoclaved DI water; LB agar media were used to enumerate
557 colony-forming units (CFUs) (Amato et al., 2013; Keren, Kaldalu, et al., 2004; Orman &
558 Brynildsen, 2015). For washing cells and removing chemicals and antibiotics before plating on
559 agar media, 1X Phosphate-Buffered Saline (PBS) was employed. In the persister assay,
560 concentrations of 5 µg/mL of ofloxacin (OFX), 200 µg/mL of ampicillin (AMP), and 50 µg/mL of
561 gentamicin (GEN) were used (Allison et al., 2011; De Groote et al., 2009; Keren, Kaldalu, et al.,
562 2004; Keren, Shah, et al., 2004). The retention of plasmids necessitated 50 µg/mL of kanamycin
563 (KAN) in the culture media (Orman & Brynildsen, 2015). Fluorescent protein expression was
564 induced using 1 mM IPTG (Orman & Brynildsen, 2015). Overnight pre-cultures were prepared in
565 14 mL Falcon test tubes containing 2 mL of LB medium, inoculated from a 25% glycerol cell stock
566 stored at -80°C, and incubated for 24 hours at 37°C with shaking at 250 revolutions per minute
567 (rpm). Main cultures were established by diluting the overnight pre-cultures at a ratio of 1:1000
568 into 2 mL fresh LB medium in 14 mL Falcon test tubes. Experimental cell cultures were prepared
569 by further dilution of the main cultures into either 25 mL fresh LB medium in 250 mL baffled
570 flasks or 2 mL fresh LB medium in 14 mL Falcon test tubes. Cultures at t=5 h and t=24 h were
571 defined as early and late stationary phase cultures, respectively. Detailed experimental
572 procedures are outlined below.

573 **Cell growth and persister assays**

574 Main cultures were prepared by diluting the overnight pre-cultures at a ratio of 1:1000 into 2
575 mL of fresh LB medium in 14 mL Falcon test tubes. These cultures were then incubated at 37°C
576 with shaking at 250 rpm. Cell growth was monitored by measuring the optical density at 600 nm
577 wavelength (OD_{600}) using a Varioskan LUX Multimode Microplate Reader (Thermo Fisher,
578 Waltham, MA, USA). The plate reader data was collected using SkanIt Software V 5.0. Cell
579 cultures at both early and late stationary phases were collected from the test tubes and
580 transferred to the baffled flasks to achieve ~$5x10^7$ cells/mL. This concentration represents an
581 approximately 100-fold dilution of the WT main culture into a fresh medium within the flask. It
582 is important to highlight that we consistently employed flow cytometry to quantify the initial
583 cell count (refer to the section "Monitoring cell division" for comprehensive details). As needed,
584 adjustments in cell number-to-volume were executed to ensure the same cell number among
585 both WT and mutant strains. These cultures were then treated with antibiotics at the indicated
586 concentrations and were cultured with shaking at 37°C for 20 hours. After treatment, a 1 mL
587 sample from each flask was transferred to a microcentrifuge tube for a rigorous washing
588 protocol to minimize antibiotic carryover. The samples were centrifuged at 13,300 RPM (17,000
589 × g) for 3 minutes, and >950 µL of supernatant was carefully removed without disturbing the
590 pellet. The pellet was then resuspended in 950 µL of PBS, achieving a >20-fold dilution of
591 residual antibiotics. This wash step was repeated once more, resulting in a cumulative >400-fold
592 dilution. After the final wash, cells were resuspended in 100 µL of PBS. A 10 µL aliquot of this

593 suspension was serially diluted in a 96-well round-bottom plate, and 10 µL from each dilution
594 was spotted onto an agar plate. The remaining 90 µL of the sample was also plated to quantify
595 CFU levels around the limit of detection, (~1 CFU/mL). Plates were incubated at 37 °C for 16
596 hours (or up to 48 hours) to allow CFUs to develop. When necessary, this washing procedure
597 was repeated up to six times to assess its impact on CFU recovery.

598 **Mid-exponential phase persister assays**

599 Overnight cultures of *E. coli* K-12 MG1655 or BW25113 WT, and mutant strains were diluted
600 1:100 in 2 mL of LB medium in 14 mL Falcon tubes and incubated at 37°C with shaking at 250
601 rpm. At mid-exponential phase (OD_{600}~0.25), cells were challenged with the indicated
602 antibiotics and concentrations. At designated time points, cells (1 mL) were collected, washed
603 with 1X PBS, and plated on agar to determine colony-forming units (CFU). To quantify the initial
604 cell count, 10 µL of the culture before treatments was serially diluted and plated on LB agar. CFU
605 levels were assessed after incubating the plates for at least 16 hours at 37°C.

606 **cAMP profile assay**

607 An overnight pre-culture of *E. coli* K-12 MG1655 WT was prepared in test tubes with 2 mL of LB
608 medium. The culture was incubated at 37°C with shaking at 250 rpm for 24 hours. For the
609 experimental cultures, a 1:1000 dilution was made in fresh medium. At time-points 0, 2, 4, 6, 8
610 and 24 h, 100 µL of the experimental culture was washed with cold 1X PBS. After centrifuging at
611 13,300 rpm (17,000 x gravitational force or g), the supernatant was removed. The cells were
612 then resuspended in 100 µL of cell lysis buffer from the Cyclic AMP XP® Assay Kit (Catalog#
613 4339S, Cell Signaling Technology, Danvers, MA, USA) on ice for 10 minutes. Next, 50 µL of lysed
614 cells was mixed with the kit's horseradish peroxidase (HRP)-linked cAMP solution in the cAMP
615 assay plate. This mixture was incubated at room temperature for 3 hours on a plate shaker at
616 250 rpm. Following the 3-hour incubation, the plate content was discarded, and the plate was
617 washed four times with the kit's Wash Buffer. Then, 100 µL of tetramethylbenzidine (TMB)
618 substrate was added to allow color development, and after 30 minutes, 100 µL of the stop
619 solution provided by the kit was added. The absorbance was measured at 450 nm using a plate
620 reader. The standard curve was prepared using the same conditions and the standard cAMP
621 solutions provided by the kit to determine cAMP concentrations.

622 **Metabolomics**

623 Metabolites from both Δ*crp* and WT cells were analyzed at the Metabolon, Inc., facility
624 (Morrisville, NC, USA). Cells were cultured until the early stationary phase and late stationary
625 phase at 37°C with shaking at 250 rpm. Afterward, cells were collected through centrifugation at
626 4700 rpm at 37°C for 15 minutes, yielding a pellet of approximately 100 µL containing around
627 10^{10} cells. Subsequently, the cells were washed once with 1X PBS and then centrifuged (13,000
628 rpm, 3 minutes at 4°C). Following this, they were frozen in an ethanol/dry ice bath for 10
629 minutes. The extracts from both mutant and WT cells were subjected to analysis using ultra-
630 high-performance liquid chromatography-tandem accurate mass spectrometry (MS), a process
631 aimed at identifying a wide range of metabolites. Sample extraction, preparation, instrument
632 settings, and conditions for the MS platform adhered to Metabolon's protocols (as detailed in
633 our previous study) (Mohiuddin et al., 2022). To identify the sample's metabolites among

634 potential false positives from instrument noise, process artifacts, and redundant ion features,
635 the results were cross-referenced with Metabolon's extensive metabolite library (standards).
636 Data normalization was carried out based on protein concentration, determined using the
637 Bradford assay. The significant difference between mutant and WT was identified using Welch's
638 two-sample t-test. Further analysis involved pathway enrichment assessment using
639 MetaboAnalyst (Lu et al., 2023). This involved inputting the upregulated and downregulated
640 metabolites based on chosen thresholds. A comprehensive overview of metabolite
641 measurements, pathway enrichment, statistical analyses, and data representations can be
642 found in our previously published study (Mohiuddin et al., 2022).

643 **Proteomics**

644 Overnight cultures for both *E. coli* K-12 MG1655 WT and Δ*crp* strains were prepared using 2 mL
645 of LB medium. Incubation was carried out at 37°C and 250 rpm for 24 hours. The following day,
646 the main cultures were established under the same conditions, using a 1000-fold dilution of the
647 overnight culture in 2 mL fresh LB medium. After 24 hours, the OD_{600} of both WT and mutant
648 strains was measured and adjusted to an OD_{600} of 2.5. For further processing, 2 mL of the main
649 culture was washed twice with cold 1X PBS, maintaining the cold environment throughout.
650 Centrifugation conditions were set at 4°C, 13,000 rpm for 3 minutes. Before the final
651 centrifugation, a cell count was conducted using flow cytometry. This involved using 10 µL of
652 washed culture and 990 µL of 1X PBS. Subsequent to centrifugation, the pellets were collected.
653 Cell lysis was carried out using 300 µL of NEBExpress® *E. coli* Lysis Reagent (Catalog# P8116S,
654 Ipswich, MA, USA) at room temperature for 30 minutes. Following this, the lysed samples were
655 centrifuged at 16,600 x g for 10 minutes, and 250 µL of supernatants were collected from each
656 sample for the assay. The total protein concentration of the supernatants was determined using
657 the bicinchoninic acid (BCA) assay (Catalog# 23225, Thermo Fisher Scientific, Waltham, MA,
658 USA). In a 96-well plate, 25 µL of each cell lysate sample, diluted 5 and 10 times with ultra-pure
659 DI water, were loaded into each well. Subsequently, 200 µL of the BCA working reagent (50:1,
660 Reagent A:B) was added to each well and mixed on a plate shaker for 30 seconds. The plate was
661 then incubated at 37°C for 30 minutes, followed by cooling for 5 minutes at room temperature,
662 shielded from light. The absorbance was finally measured at 562 nm using a plate reader, and
663 the total protein concentration in each sample was calculated using a standard curve prepared
664 from standard protein solutions. Protein analysis for both WT and mutant was conducted by the
665 proteomics service at UT Health's Clinical and Translational Proteomics Service Center (Houston,
666 TX). The samples underwent acetone precipitation, during which proteins were precipitated by
667 exposing them to -20°C for 3 hours. Following this, a centrifugation step at 12,000 x g for 5
668 minutes separated the precipitated pellets. These pellets were subsequently subjected to
669 denaturation and reduction using a mixture containing 30 µL of 6 M urea, 20 mM DTT in 150
670 mM Tris HCl (pH 8.0) at 37°C for 40 minutes. Afterward, alkylation was carried out with 40 mM
671 iodoacetamide in the absence of light for 30 minutes. To prepare for digestion, the reaction
672 mixture was diluted 10-fold using 50 mM Tris-HCl (pH 8.0) and then incubated overnight at 37°C
673 with trypsin at a 1:30 enzyme-to-substrate ratio. The digestion process was terminated by
674 adding an equal volume of 2% formic acid, followed by desalting using Waters Oasis HLB 1 mL

675 reverse phase cartridges, following the vendor's recommended procedure. Finally, the elutes
676 were dried using vacuum centrifugation. Approximately 1 µg of the tryptic digest, prepared in a
677 solution containing 2% acetonitrile and 0.1% formic acid in water, underwent analysis using
678 LC/MS/MS. The instrument used was the Orbitrap Fusion™ Tribrid™ mass spectrometer by
679 Thermo Scientific™, connected to a Dionex UltiMate 3000 Binary RSLCnano System. The
680 separation of peptides occurred on an analytical C18 column with dimensions of 100 µm ID x 25
681 cm, featuring 5 µm particles and an 18 Å pore size. Peptides were eluted at a flow rate of 350
682 nL/min. The gradient conditions applied were as follows: a gradient starting from 3% B and
683 increasing to 22% B over a duration of 90 minutes, followed by a step to 22%-35% B for 10
684 minutes, then another step to 35%-90% B for 10 minutes, and finally, maintaining 90% B for an
685 additional 10 minutes (Solvent A was composed of 0.1% formic acid in water, while solvent B
686 contained 0.1% formic acid in acetonitrile). The peptides were analyzed using a data-dependent
687 acquisition method. The Orbitrap Fusion MS operated by measuring FTMS1 spectra with a
688 resolution of 120,000 FWHM, scanning in the m/z range of 350-1500, using an AGC target set to
689 2E5, and with a maximum injection time of 50 ms. Within a maximum cycle time of 3 sec, ITMS2
690 spectra were collected in rapid scan mode. High Collision Dissociation (HCD) was employed with
691 a normalized collision energy (NCE) of 34, an isolation window of 1.6 m/z, an AGC target set to
692 1E4, and a maximum injection time of 35 ms. Dynamic exclusion was implemented for a
693 duration of 35 sec to prevent repeated analysis of the same ions. For the experimental analysis,
694 the Thermo Scientific™ Proteome Discoverer™ software version 1.4 was utilized to process the
695 raw data files. The spectra were subjected to analysis against the *E. coli* proteome database
696 (Swiss-Prot 29,161) through the Sequest HT search engine. Additionally, the spectra were
697 compared against a decoy database, employing a target false discovery rate (FDR) of 1% for
698 stringent criteria and 5% for more relaxed criteria. The enzymatic cleavage allowance for trypsin
699 included up to two potential missed cleavages. The MS tolerance was defined as 10 ppm, while
700 the MS/MS tolerance was set at 0.6 Da. Fixed modification involved carbamidomethylation on
701 cysteine residues, and variable modifications encompassed methionine oxidation and
702 asparagine deamidation. For proteomics data processing and fold change calculations, the
703 approaches were essentially followed by the method paper from Aguilan et al. (Aguilan et al.,
704 2020). Then, the STRING tool V12.0 (Szklarczyk et al., 2021, 2023) was employed to find the
705 significant networks among input proteins. To generate the protein network and pathway
706 enrichment analysis, we input the protein identifiers (Accession numbers) for upregulated or
707 downregulated proteins with at least a 2-fold increase or reduction, respectively. *E. coli* K-12
708 was selected as the organism of interest. We opted for evidence as the criterion for network
709 edges, prioritizing the type of interaction evidence, helping us conduct an automated pathway-
710 enrichment analysis, centering on the entered proteins and identifying pathways that occurred
711 more frequently than expected. This analysis was grounded in the statistical background of the
712 entire genome and encompasses various functional pathway classification frameworks, such as
713 Gene Ontology annotations, KEGG pathways, and Uniprot keywords, as detailed elsewhere
714 (Szklarczyk et al., 2021, 2023). In pathway enrichment analysis, the "strength score," calculated
715 as Log_{10}(observed/expected), serves to assess the degree or significance of enrichment within a

716 specific biological pathway. This metric reflects the magnitude of the enrichment effect, with a
717 higher score indicating stronger enrichment. The score is derived from the ratio of i) annotated
718 proteins in the network for a given term to ii) the expected number of proteins annotated with
719 the same term in a random network of equivalent size (Szklarczyk et al., 2021, 2023). To gauge
720 the significance of enrichment, False Discovery Rate (FDR) is employed. FDR scores represent p-
721 values corrected for multiple testing within each category using the Benjamini–Hochberg
722 procedure (Szklarczyk et al., 2021, 2023).

723 **Monitoring cell division**

724 To monitor cell division and quantify non-growing cells, we utilized inducible fluorescent protein
725 (mCherry) expression. Overnight pre-cultures of *E. coli* MO were prepared with 2 mL of LB
726 medium containing 1 mM of IPTG. These cultures were grown in test tubes at 37°C with shaking
727 at 250 rpm for 24 hours. Main cultures were established by diluting the overnight pre-cultures
728 (at a ratio of 1:1000) into 2 mL of fresh LB medium in 14 mL Falcon test tubes. These cultures
729 were incubated at 37°C with shaking at 250 rpm. Cells were allowed to grow until they reached
730 the early stationary phase and the late stationary phase. The mCherry positive cells were then
731 collected, washed twice with 1X PBS to remove the IPTG from the culture, and subsequently re-
732 suspended in fresh 2 ml LB media in test tubes to achieve ~$5x10^7$ cells/mL. This concentration
733 represents an approximately 100-fold dilution. When needed, adjustments in cell number-to-
734 volume were made to ensure the same cell number among both WT and mutant strains. In the
735 experimental culture test tubes, 2 mL of LB medium was added, and the volume of washed cells
736 was inoculated to achieve an OD_{600} of 0.0286. The culture was then incubated at 37°C with
737 shaking at 250 rpm. At specific time points (0, 1, 2, and 2.5 h), cells were collected and re-
738 suspended in 1X PBS to measure their fluorescent protein content using flow cytometry. For
739 flow cytometry analysis, cells were collected and diluted to a desired cell density (~10^6-10^7
740 cells/mL) in 1 mL of 1X PBS in flow cytometry tubes (5 mL round-bottom Falcon tubes, size: 12 x
741 75 mm). The flow cytometry analysis was conducted using a NovoCyte 3000RYB instrument
742 (ACEA Bioscience Inc., San Diego, CA, USA). During flow cytometry analysis, a slow sample flow
743 rate of 14 µL/min was chosen, along with a sample stream diameter (core diameter) of 7.7 µm.
744 The instrument maintained a constant sheath flow rate of 6.5 mL/min. The core diameter was
745 calculated using the ratio of the sample flow rate to the sheath flow rate. These specific
746 conditions were selected to achieve improved data resolution for the size of *E. coli* cells. Flow
747 diagrams utilized forward and side scatter signals from viable cells, alongside a control of
748 solvent devoid of cells, to ascertain the presence of cells. For the flow cytometry analysis, cells
749 were excited at a 561 nm wavelength, and the red fluorescence was detected using a 615/20
750 nm bandpass filter.

751 **Flow Cytometry Analysis of Cell Growth**

752 Overnight cultures of *E. coli* K-12 MG1655 MO WT and mutant strains were diluted at a ratio of
753 1:1000 into 2 mL of fresh LB medium, placed in 14 mL Falcon test tubes, and incubated at 37°C
754 with shaking at 250 rpm for 24 hours. For the main cultures, a similar strategy was employed.
755 The cultures were diluted at a ratio of 1:100 into 2 mL of fresh LB medium in 14 mL Falcon test
756 tubes. These cultures were then incubated at 37°C with shaking at 250 rpm. At specific time

757 points, including t=0, 20 min, 40 min, and 1 to 5 h, the cell growth was halted. This was
758 achieved by diluting the cells in 1X PBS containing 25 µg/mL of chloramphenicol (CAM). The
759 CAM treatment allowed for subsequent analysis without further division. Flow cytometry was
760 then utilized to measure the number of cells at each of these time points. This approach
761 provided insight into cell division dynamics and allowed for the quantification of cell
762 populations under specific conditions.

763 **Fluorescent protein expression assay for reporter genes**

764 Mutant and control strains were derived from *E. coli* K-12 MG1655 and carried pMSs201-*gfp*
765 plasmids incorporating $P_{sdhABCD}$ or P_{cyaA} gene promoters. Overnight pre-cultures were prepared
766 using 2 mL of LB medium supplemented with 50 µg/mL KAN. These cultures were incubated in
767 test tubes within a shaker at 37°C for 24 hours. Main cultures were established by diluting the
768 overnight pre-cultures at a ratio of 1:1000 into 2 mL of fresh LB medium within 14 mL Falcon
769 test tubes. These main cultures were maintained at 37°C with shaking at 250 rpm. Cell cultures
770 at the desired growth phase were collected and then diluted to attain a desired cell density of
771 around 10^6-10^7 cells/mL in 1 mL of 1X PBS within flow cytometry tubes. This allowed for
772 subsequent flow cytometry analysis, using the same conditions as described earlier for
773 monitoring cell division (refer to "Monitoring cell division"). During analysis, a laser emitting
774 light at 488 nm was used to excite the cells, and the resulting green fluorescence was detected
775 using a 530/30 nm bandpass filter. This setup enabled the examination of the fluorescence
776 patterns of the cells, offering insights into their dynamics under different conditions.

777 **Redox Sensor Green assay**

778 To gauge bacterial metabolic activity, we employed the Redox Sensor Green (RSG) dye from
779 Thermo Fisher (Catalog# B34954, Thermo Fisher Scientific, Waltham, MA). *E. coli* K-12 MG1655
780 WT and mutant cells from the desired growth phase were diluted at a ratio of 1:100 in 1 mL of
781 1X PBS. To this solution, 1 µL of the RSG dye was added to flow cytometry tubes. After a brief
782 vortexing to ensure uniform mixing, the samples were incubated at 37°C in darkness for 10
783 minutes. Subsequently, these samples were subjected to flow cytometry analysis. For the flow
784 cytometry analysis, the same methodology as employed in "Monitoring cell division" was
785 followed, with one variation. Cells were excited at 488 nm during analysis, and the resulting
786 green fluorescence was detected using a 530/30 nm bandpass filter. This setup allowed us to
787 assess the fluorescence patterns, reflecting the metabolic activity of the bacterial cells under
788 different conditions. As a control measure, cells were treated with 20 µM of carbonyl cyanide
789 m-chlorophenyl hydrazone (CCCP) for 5 minutes before the addition of the RSG dye. This served
790 to validate the assay's sensitivity to changes in metabolic activity (**Figure 5–figure supplement**
791 **1**).

792 **Metabolic activity of non-lysing cells and VBNC cell quantification**

793 Overnight cultures of *E. coli* K-12 MG1655 MO WT and mutant strains were diluted at a ratio of
794 1:1000 into 2 mL of fresh LB medium supplemented with 1 mM IPTG. These cultures were
795 established in 14 mL Falcon test tubes and incubated at 37°C with shaking at 250 rpm for 24
796 hours. Treatment cultures were prepared by diluting the main cultures at a ratio of 1:100 into
797 25 mL of fresh LB medium supplemented with 1 mM IPTG. These cultures were set up in 250 mL

798 baffled flasks and contained 200 µg/mL AMP. They were then cultured at 37°C with shaking at
799 250 rpm for 20 hours. Both before and after the treatment, 1 mL samples were collected from
800 the cultures. These samples were subjected to a washing procedure with 1X PBS to eliminate
801 the antibiotic present in the samples. The washed cells were then resuspended in 1 mL of 1X
802 PBS within flow cytometry tubes. To measure the metabolic activity of the non-lysing cells, the
803 RSG dye was employed as described above. Intact cells (following antibiotic treatment), stained
804 as live with RSG, comprised both persister and VBNC cells. Persister levels were quantified by
805 plating the cells on an agar medium, as described previously (Orman & Brynildsen, 2013b). As
806 VBNC cells cannot grow on agar medium, their enumeration involved subtracting the number of
807 persister cells from the total number of intact cells.

808 **Screening *E. coli* (K-12 BW25113) Keio Knockout Collection**

809 Overnight cultures of individual mutant strains, along with their parental strain K-12 BW25113
810 WT harboring a kanamycin-resistant marker, were diluted at a ratio of 1:1000 in fresh LB
811 medium containing 50 µg/mL of KAN. This was done in 14 mL Falcon test tubes and the cultures
812 were then incubated at 37°C with shaking at 250 rpm. Upon reaching the late stationary phase,
813 cells were further diluted at a ratio of 1:100 in fresh medium supplemented with antibiotics at
814 specified concentrations. These cultures were once again incubated at 37°C with shaking for 20
815 hours. Following the 20-hour treatment period, the same methodology described in the section
816 "Cell growth and persister assays" was employed to quantify the number of persisters. This
817 approach allowed for an assessment of the impact of antibiotics on the formation of persister
818 cells for both mutant strains and the parental K-12 BW25113 WT strain.

819 **Persister quantitation in *E. coli* K-12 MG1655 single gene deletions**

820 Overnight cultures of mutant strains were diluted at a ratio of 1:1000 in 14 mL Falcon test tubes
821 containing 2 mL of LB medium. These cultures were then incubated at 37°C with shaking at 250
822 rpm. Upon reaching the late stationary phase, cells were diluted at a ratio of 1:100 in fresh
823 medium supplemented with antibiotics at specified concentrations. The cultures were once
824 again subjected to shaking at 37°C for 20 hours. The same method described earlier, referred to
825 as "Cell growth and persister assays," was employed to quantify the number of persister cells
826 resulting from this treatment. This approach allowed for the assessment of the impact of
827 antibiotic exposure on persister cell formation within the mutant strains.

828 **Statistics and reproducibility**

829 A nonlinear logarithmic model was employed to create biphasic kill curves (Mohiuddin, Hoang,
830 et al., 2020; Windels et al., 2019). The significance of these kill curves was determined through
831 the utilization of F-statistics (Mohiuddin, Hoang, et al., 2020; Windels et al., 2019).
832 Metabolomics data were subjected to analysis using Welch's two-sample t-test in order to
833 identify metabolites that significantly differed between the control and mutant groups (YUEN,
834 1974). For all experiments, a minimum of three independent biological replicates were
835 conducted, unless explicitly stated otherwise. In each figure (excluding flow diagrams), the data
836 for each time point are represented as the mean value accompanied by the standard deviation.
837 In terms of statistical significance analysis, the designated threshold values for P were set as
838 follows: *P < 0.05, **P < 0.01, ***P < 0.001, and ****P < 0.0001. All figures were generated

using GraphPad Prism 10.3.0. The statistical analyses were carried out using the statistical functions of GraphPad Prism 10.3.0. For the clustering of metabolomics and proteomics data, the "Clustergram" function of MATLAB (V R2020b) was employed. FlowJo (V 10.8.1) was the tool used to analyze the data acquired from flow cytometry.

Data Availability

All data generated or analyzed during this study are included in the manuscript and supporting files.

Article and author information

Author details

Han G Ngo
Cullen College of Engineering, William A. Brookshire Department of Chemical and Biomolecular Engineering, University of Houston, Houston, United States
Contribution: Conception and design, Acquisition of data, Analysis and interpretation of data, Drafting or revising the article
Competing interests: No competing interests declared
Sayed G Mohiuddin
Cullen College of Engineering, William A. Brookshire Department of Chemical and Biomolecular Engineering, University of Houston, Houston, United States
Contribution: Acquisition of data, Analysis and interpretation of data, Drafting or revising the article
Competing interests: No competing interests declared
Aina Ananda
School of Science, Department of Biology, Monmouth University, West Long Branch, United States
Contribution: Analysis of proteomics data, Drafting or revising the article
Competing interests: No competing interests declared
Mehmet A Orman
Cullen College of Engineering, William A. Brookshire Department of Chemical and Biomolecular Engineering, University of Houston, Houston, United States
Contribution: Conception and design, Acquisition of data, Analysis and interpretation of data, Drafting or revising the article
For correspondence: morman@central.uh.edu
Competing interests: No competing interests declared

Funding

National Science Foundation (2044375)

- Mehmet A Orman

National Institutes of Health (R01AI143643)

- Mehmet A Orman

The funders had no role in study design, data collection and interpretation, or the decision to submit the work for publication.

Acknowledgements

We would like to express our gratitude to the members of Dr. Orman's laboratory for their support and assistance throughout this study. We also thank Metabolon, Inc. for their expertise in metabolomics experiments and data analysis, as well as UT Health's Clinical and Translational Proteomics Service Center for their contribution to the proteomics experiments.

References

Adams, K. N., Takaki, K., Connolly, L. E., Wiedenhoft, H., Winglee, K., Humbert, O., Edelstein, P. H., Cosma, C. L., & Ramakrishnan, L. (2011). Drug tolerance in replicating mycobacteria mediated by a macrophage-induced efflux mechanism. *Cell*, *145*(1), 39–53. https://doi.org/10.1016/j.cell.2011.02.022

Aguilan, J. T., Kulej, K., & Sidoli, S. (2020). Guide for protein fold change and *p* -value calculation for non-experts in proteomics. *Molecular Omics*, *16*(6), 573–582. https://doi.org/10.1039/D0MO00087F

Aiba, H. (1985). Transcription of the Escherichia coli adenylate cyclase gene is negatively regulated by cAMP-cAMP receptor protein. *The Journal of Biological Chemistry*, *260*(5), 3063–3070.

Allison, K. R., Brynildsen, M. P., & Collins, J. J. (2011). Metabolite-enabled eradication of bacterial persisters by aminoglycosides. *Nature*, *473*(7346), 216–220. https://doi.org/10.1038/nature10069

Amato, S. M., Fazen, C. H., Henry, T. C., Mok, W. W. K., Orman, M. A., Sandvik, E. L., Volzing, K. G., & Brynildsen, M. P. (2014). The role of metabolism in bacterial persistence. *Frontiers in Microbiology*, *5*, 70.

Amato, S. M., Orman, M. A., & Brynildsen, M. P. (2013). Metabolic Control of Persister Formation in Escherichia coli. *Molecular Cell*, *50*(4), 475–487. https://doi.org/10.1016/J.MOLCEL.2013.04.002

Arnoldini, M., Vizcarra, I. A., Peña-Miller, R., Stocker, N., Diard, M., Vogel, V., Beardmore, R. E., Hardt, W.-D., & Ackermann, M. (2014). Bistable Expression of Virulence Genes in Salmonella Leads to the Formation of an Antibiotic-Tolerant Subpopulation. *PLoS Biology*, *12*(8), e1001928. https://doi.org/10.1371/journal.pbio.1001928

Ayrapetyan, M., Williams, T., & Oliver, J. D. (2018). Relationship between the Viable but Nonculturable State and Antibiotic Persister Cells. *Journal of Bacteriology*, *200*(20). https://doi.org/10.1128/JB.00249-18

Baba, T., Ara, T., Hasegawa, M., Takai, Y., Okumura, Y., Baba, M., Datsenko, K. A., Tomita, M., Wanner, B. L., & Mori, H. (2006). Construction of *Escherichia coli* K-12 in-frame, single-gene knockout mutants: the Keio collection. *Molecular Systems Biology*, *2*(1). https://doi.org/10.1038/msb4100050

Balaban, N. Q., Merrin, J., Chait, R., Kowalik, L., & Leibler, S. (2004). Bacterial persistence as a phenotypic switch. *Science*, *305*(5690), 1622–1625. https://doi.org/10.1126/SCIENCE.1099390

Barrett, T. C., Mok, W. W. K., Murawski, A. M., & Brynildsen, M. P. (2019). Enhanced antibiotic resistance development from fluoroquinolone persisters after a single exposure to antibiotic. *Nature Communications*, *10*(1), 1177.

Bettenbrock, K., Sauter, T., Jahreis, K., Kremling, A., Lengeler, J. W., & Gilles, E.-D. (2007). Correlation between growth rates, EIIACrr phosphorylation, and intracellular cyclic AMP levels in Escherichia coli K-12. *Journal of Bacteriology*, *189*(19), 6891–6900.

Chu, W., Zere, T. R., Weber, M. M., Wood, T. K., Whiteley, M., Hidalgo-Romano, B., Valenzuela Jr, E., & McLean, R. J. C. (2012). Indole production promotes Escherichia coli mixed-culture growth with Pseudomonas aeruginosa by inhibiting quorum signaling. *Applied and Environmental Microbiology*, *78*(2), 411–419.

Conlon, B. P., Rowe, S. E., Gandt, A. B., Nuxoll, A. S., Donegan, N. P., Zalis, E. A., Clair, G., Adkins, J. N., Cheung, A. L., & Lewis, K. (2016). Persister formation in Staphylococcus aureus is associated with ATP depletion. *Nature Microbiology*, *1*(5), 1–7.

Cunningham, L., & Guest, J. R. (1998). Transcription and transcript processing in the sdhCDAB-sucABCD operon of Escherichia coli. *Microbiology (Reading, England)*, *144 (Pt 8)*, 2113–2123. https://doi.org/10.1099/00221287-144-8-2113

Datsenko, K. A., & Wanner, B. L. (2000). One-step inactivation of chromosomal genes in *Escherichia coli* K-12 using PCR products. *Proceedings of the National Academy of Sciences*, *97*(12), 6640–6645. https://doi.org/10.1073/pnas.120163297

De Groote, V. N., Verstraeten, N., Fauvart, M., Kint, C. I., Verbeeck, A. M., Beullens, S., Cornelis, P., & Michiels, J. (2009). Novel persistence genes in *Pseudomonas aeruginosa* identified by high-throughput screening. *FEMS Microbiology Letters*, *297*(1), 73–79. https://doi.org/10.1111/j.1574-6968.2009.01657.x

Deutscher, J. (2008). The mechanisms of carbon catabolite repression in bacteria. *Current Opinion in Microbiology*, *11*(2), 87–93.

Fic, E., Bonarek, P., Górecki, A., Kedracka-Krok, S., Mikolajczak, J., Polit, A., Tworzydlo, M., Dziedzicka-Wasylewska, M., & Wasylewski, Z. (2009). cAMP receptor protein from Escherichia coli as a model of signal transduction in proteins–a review. *Microbial Physiology*, *17*(1), 1–11.

Fisher, R. A., Gollan, B., & Helaine, S. (2017). Persistent bacterial infections and persister cells. *Nature Reviews Microbiology*, *15*(8), 453–464. https://doi.org/10.1038/nrmicro.2017.42

Gonzalez-Gil, G. (1998). Regulation of crp transcription by oscillation between distinct nucleoprotein complexes. *The EMBO Journal*, *17*(10), 2877–2885. https://doi.org/10.1093/emboj/17.10.2877

Goormaghtigh, F., & Van Melderen, L. (2019). Single-cell imaging and characterization of Escherichia coli persister cells to ofloxacin in exponential cultures. *Science Advances*, *5*(6), eaav9462.

Görke, B., & Stülke, J. (2008). Carbon catabolite repression in bacteria: many ways to make the most out of nutrients. *Nature Reviews Microbiology*, *6*(8), 613–624.

Gosset, G., Zhang, Z., Nayyar, S., Cuevas, W. A., & Saier, M. H. (2004). Transcriptome Analysis of Crp-Dependent Catabolite Control of Gene Expression in *Escherichia coli*. *Journal of Bacteriology*, *186*(11), 3516–3524. https://doi.org/10.1128/JB.186.11.3516-3524.2004

Hanahan, D., & Weinberg, R. A. (2011). Hallmarks of cancer: the next generation. *Cell*, *144*(5), 646–674.

966 Hofsteenge, N., van Nimwegen, E., & Silander, O. K. (2013). Quantitative analysis of persister
967 fractions suggests different mechanisms of formation among environmental isolates of E.
968 coli. *BMC Microbiology*, *13*(1), 25. https://doi.org/10.1186/1471-2180-13-25
969 Hossain, T., Singh, A., & Butzin, N. C. (2023). *Escherichia coli* cells are primed for survival before
970 lethal antibiotic stress. *Microbiology Spectrum*, *11*(5).
971 https://doi.org/10.1128/spectrum.01219-23
972 Huemer, M., Mairpady Shambat, S., Brugger, S. D., & Zinkernagel, A. S. (2020). Antibiotic
973 resistance and persistence—Implications for human health and treatment perspectives.
974 *EMBO Reports*, *21*(12). https://doi.org/10.15252/embr.202051034
975 Joers, A., Kaldalu, N., & Tenson, T. (2010). The frequency of persisters in Escherichia coli reflects
976 the kinetics of awakening from dormancy. *Journal of Bacteriology*, *192*(13), 3379–3384.
977 Jõers, A., & Tenson, T. (2016). Growth resumption from stationary phase reveals memory in
978 Escherichia coli cultures. *Scientific Reports*, *6*(1), 24055.
979 https://doi.org/10.1038/srep24055
980 Kaldalu, N., & Tenson, T. (2019). Slow growth causes bacterial persistence. *Science Signaling*,
981 *12*(592). https://doi.org/10.1126/scisignal.aay1167
982 Keren, I., Kaldalu, N., Spoering, A., Wang, Y., & Lewis, K. (2004). Persister cells and tolerance to
983 antimicrobials. *FEMS Microbiology Letters*, *230*(1), 13–18.
984 Keren, I., Shah, D., Spoering, A., Kaldalu, N., & Lewis, K. (2004). Specialized Persister Cells and
985 the Mechanism of Multidrug Tolerance in *Escherichia coli*. *Journal of Bacteriology*, *186*(24),
986 8172–8180. https://doi.org/10.1128/JB.186.24.8172-8180.2004
987 Keseler, I. M. (2004). EcoCyc: a comprehensive database resource for Escherichia coli. *Nucleic*
988 *Acids Research*, *33*(Database issue), D334–D337. https://doi.org/10.1093/nar/gki108
989 Keseler, I. M., Collado-Vides, J., Santos-Zavaleta, A., Peralta-Gil, M., Gama-Castro, S., Muniz-
990 Rascado, L., Bonavides-Martinez, C., Paley, S., Krummenacker, M., Altman, T., Kaipa, P.,
991 Spaulding, A., Pacheco, J., Latendresse, M., Fulcher, C., Sarker, M., Shearer, A. G., Mackie,
992 A., Paulsen, I., … Karp, P. D. (2011). EcoCyc: a comprehensive database of Escherichia coli
993 biology. *Nucleic Acids Research*, *39*(Database), D583–D590.
994 https://doi.org/10.1093/nar/gkq1143
995 Khankal, R., Chin, J. W., Ghosh, D., & Cirino, P. C. (2009). Transcriptional effects of CRP*
996 expression in Escherichia coli. *Journal of Biological Engineering*, *3*(1), 13.
997 https://doi.org/10.1186/1754-1611-3-13
998 Kim, J.-S., Cho, D.-H., Heo, P., Jung, S.-C., Park, M., Oh, E.-J., Sung, J., Kim, P.-J., Lee, S.-C., Lee,
999 D.-H., Lee, S., Lee, C. H., Shin, D., Jin, Y.-S., & Kweon, D.-H. (2016). Fumarate-Mediated
1000 Persistence of Escherichia coli against Antibiotics. *Antimicrobial Agents and Chemotherapy*,
1001 *60*(4), 2232–2240. https://doi.org/10.1128/AAC.01794-15
1002 Kohanski, M. A., Dwyer, D. J., Hayete, B., Lawrence, C. A., & Collins, J. J. (2007). A Common
1003 Mechanism of Cellular Death Induced by Bactericidal Antibiotics. *Cell*, *130*(5), 797–810.
1004 https://doi.org/10.1016/j.cell.2007.06.049
1005 Kolb, A., Busby, S., Buc, H., Garges, S., & Adhya, S. (1993). Transcriptional regulation by cAMP
1006 and its receptor protein. *Annual Review of Biochemistry*, *62*(1), 749–797.
1007 Leatham-Jensen, M. P., Mokszycki, M. E., Rowley, D. C., Deering, R., Camberg, J. L., Sokurenko,
1008 E. V., Tchesnokova, V. L., Frimodt-Møller, J., Krogfelt, K. A., Leth Nielsen, K., Frimodt-
1009 Møller, N., Sun, G., & Cohen, P. S. (2016). Uropathogenic Escherichia coli Metabolite-

1010 Dependent Quiescence and Persistence May Explain Antibiotic Tolerance during Urinary
1011 Tract Infection. *MSphere*, *1*(1). https://doi.org/10.1128/mSphere.00055-15
1012 Levin-Reisman, I., Ronin, I., Gefen, O., Braniss, I., Shoresh, N., & Balaban, N. Q. (2017). Antibiotic
1013 tolerance facilitates the evolution of resistance. *Science*, *355*(6327), 826–830.
1014 Lewis, K. (2010). Persister cells. In *Annual Review of Microbiology* (Vol. 64).
1015 https://doi.org/10.1146/annurev.micro.112408.134306
1016 Li, B., Chen, X., Yang, J.-Y., Gao, S., & Bai, F. (2024). Intracellular ATP concentration is a key
1017 regulator of bacterial cell fate. *Journal of Bacteriology*, *206*(12).
1018 https://doi.org/10.1128/jb.00208-24
1019 Liu, S., Wu, N., Zhang, S., Yuan, Y., Zhang, W., & Zhang, Y. (2017). Variable Persister Gene
1020 Interactions with (p)ppGpp for Persister Formation in Escherichia coli. *Frontiers in*
1021 *Microbiology*, *8*. https://doi.org/10.3389/fmicb.2017.01795
1022 Lobritz, M. A., Belenky, P., Porter, C. B. M., Gutierrez, A., Yang, J. H., Schwarz, E. G., Dwyer, D. J.,
1023 Khalil, A. S., & Collins, J. J. (2015). Antibiotic efficacy is linked to bacterial cellular
1024 respiration. *Proceedings of the National Academy of Sciences*, *112*(27), 8173–8180.
1025 https://doi.org/10.1073/pnas.1509743112
1026 Lu, Y., Pang, Z., & Xia, J. (2023). Comprehensive investigation of pathway enrichment methods
1027 for functional interpretation of LC–MS global metabolomics data. *Briefings in*
1028 *Bioinformatics*, *24*(1), bbac553.
1029 Luidalepp, H., Joers, A., Kaldalu, N., & Tenson, T. (2011). Age of inoculum strongly influences
1030 persister frequency and can mask effects of mutations implicated in altered persistence.
1031 *Journal of Bacteriology*, *193*(14), 3598–3605.
1032 Lynch, A. S., & Lin, E. C. (1996). Transcriptional control mediated by the ArcA two-component
1033 response regulator protein of Escherichia coli: characterization of DNA binding at target
1034 promoters. *Journal of Bacteriology*, *178*(21), 6238–6249.
1035 https://doi.org/10.1128/jb.178.21.6238-6249.1996
1036 Ma, C., Sim, S., Shi, W., Du, L., Xing, D., & Zhang, Y. (2010). Energy production genes sucB and
1037 ubiF are involved in persister survival and tolerance to multiple antibiotics and stresses in
1038 Escherichia coli. *FEMS Microbiology Letters*, *303*(1), 33–40.
1039 Majerfeld, I. H., Miller, D., Spitz, E., & Rickenberg, H. V. (1981). Regulation of the synthesis of
1040 adenylate cyclase in Escherichia coli by the cAMP — cAMP receptor protein complex.
1041 *Molecular and General Genetics MGG*, *181*(4), 470–475.
1042 https://doi.org/10.1007/BF00428738
1043 Manuse, S., Shan, Y., Canas-Duarte, S. J., Bakshi, S., Sun, W.-S., Mori, H., Paulsson, J., & Lewis, K.
1044 (2021). Bacterial persisters are a stochastically formed subpopulation of low-energy cells.
1045 *PLoS Biology*, *19*(4), e3001194.
1046 Michiels, J. E., Van den Bergh, B., Verstraeten, N., & Michiels, J. (2016). Molecular mechanisms
1047 and clinical implications of bacterial persistence. *Drug Resistance Updates*, *29*, 76–89.
1048 https://doi.org/10.1016/j.drup.2016.10.002
1049 Mohiuddin, S. G., Hoang, T., Saba, A., Karki, P., & Orman, M. A. (2020). Identifying Metabolic
1050 Inhibitors to Reduce Bacterial Persistence. *Frontiers in Microbiology*, *11*.
1051 https://doi.org/10.3389/fmicb.2020.00472

1052 Mohiuddin, S. G., Kavousi, P., & Orman, M. A. (2020). Flow-cytometry analysis reveals persister
1053 resuscitation characteristics. *BMC Microbiology*, *20*(1), 202.
1054 https://doi.org/10.1186/s12866-020-01888-3
1055 Mohiuddin, S. G., Nguyen, T. V., & Orman, M. A. (2022). Pleiotropic actions of phenothiazine
1056 drugs are detrimental to Gram-negative bacterial persister cells. *Communications Biology*,
1057 *5*(1), 217.
1058 Mok, W. W. K., Orman, M. A., & Brynildsen, M. P. (2015). Impacts of global transcriptional
1059 regulators on persister metabolism. *Antimicrobial Agents and Chemotherapy*, *59*(5), 2713–
1060 2719.
1061 Mok, W. W. K., Park, J. O., Rabinowitz, J. D., & Brynildsen, M. P. (2015). RNA Futile Cycling in
1062 Model Persisters Derived from MazF Accumulation. *MBio*, *6*(6).
1063 https://doi.org/10.1128/mBio.01588-15
1064 Molina-Quiroz, R. C., Silva-Valenzuela, C., Brewster, J., Castro-Nallar, E., Levy, S. B., & Camilli, A.
1065 (2018). Cyclic AMP regulates bacterial persistence through repression of the oxidative
1066 stress response and SOS-dependent DNA repair in uropathogenic Escherichia coli. *MBio*,
1067 *9*(1), 10–1128.
1068 Murray, C. J. L., Ikuta, K. S., Sharara, F., Swetschinski, L., Robles Aguilar, G., Gray, A., Han, C.,
1069 Bisignano, C., Rao, P., Wool, E., Johnson, S. C., Browne, A. J., Chipeta, M. G., Fell, F.,
1070 Hackett, S., Haines-Woodhouse, G., Kashef Hamadani, B. H., Kumaran, E. A. P., McManigal,
1071 B., … Naghavi, M. (2022). Global burden of bacterial antimicrobial resistance in 2019: a
1072 systematic analysis. *The Lancet*, *399*(10325), 629–655. https://doi.org/10.1016/S0140-
1073 6736(21)02724-0
1074 Opalek, M., Smug, B. J., & Wloch-Salamon, D. (2022). How to determine microbial lag phase
1075 duration? *BioRxiv*, 2011–2022.
1076 Orman, M. A., & Brynildsen, M. P. (2013a). Dormancy is not necessary or sufficient for bacterial
1077 persistence. *Antimicrobial Agents and Chemotherapy*, *57*(7), 3230–3239.
1078 Orman, M. A., & Brynildsen, M. P. (2013b). Establishment of a method to rapidly assay bacterial
1079 persister metabolism. *Antimicrobial Agents and Chemotherapy*, *57*(9), 4398–4409.
1080 Orman, M. A., & Brynildsen, M. P. (2015). Inhibition of stationary phase respiration impairs
1081 persister formation in E. coli. *Nature Communications*, *6*(1), 7983.
1082 Pandey, S., Sahukhal, G. S., & Elasri, M. O. (2021). The msaABCR Operon Regulates Persister
1083 Formation by Modulating Energy Metabolism in Staphylococcus aureus. *Frontiers in*
1084 *Microbiology*, *12*. https://doi.org/10.3389/fmicb.2021.657753
1085 Park, Y.-H., Lee, B. R., Seok, Y.-J., & Peterkofsky, A. (2006). In vitro reconstitution of catabolite
1086 repression in Escherichia coli. *Journal of Biological Chemistry*, *281*(10), 6448–6454.
1087 Parsons, J. B., Sidders, A. E., Velez, A. Z., Hanson, B. M., Angeles-Solano, M., Ruffin, F., Rowe, S.
1088 E., Arias, C. A., Fowler, V. G., Thaden, J. T., & Conlon, B. P. (2024). In-patient evolution of a
1089 high-persister Escherichia coli strain with reduced in vivo antibiotic susceptibility.
1090 *Proceedings of the National Academy of Sciences of the United States of America*, *121*(3).
1091 https://doi.org/10.1073/pnas.2314514121
1092 Pastan, I., & Perlman, R. (1970). Cyclic Adenosine Monophosphate in Bacteria: In many bacteria
1093 the synthesis of inducible enzymes requires this cyclic nucleotide. *Science*, *169*(3943), 339–
1094 344.

1095 Perrenoud, A., & Sauer, U. (2005). Impact of Global Transcriptional Regulation by ArcA, ArcB,
1096 Cra, Crp, Cya, Fnr, and Mlc on Glucose Catabolism in *Escherichia coli*. *Journal of*
1097 *Bacteriology*, *187*(9), 3171–3179. https://doi.org/10.1128/JB.187.9.3171-3179.2005
1098 Porporato, P. E., Filigheddu, N., Pedro, J. M. B.-S., Kroemer, G., & Galluzzi, L. (2018).
1099 Mitochondrial metabolism and cancer. *Cell Research*, *28*(3), 265–280.
1100 Prax, M., & Bertram, R. (2014). Metabolic aspects of bacterial persisters. *Frontiers in Cellular*
1101 *and Infection Microbiology*, *4*, 148.
1102 Quail, M. A., Haydon, D. J., & Guest, J. R. (1994). The pdhR-aceEF-lpd operon of Escherichia coli
1103 expresses the pyruvate dehydrogenase complex. *Molecular Microbiology*, *12*(1), 95–104.
1104 https://doi.org/10.1111/j.1365-2958.1994.tb00998.x
1105 Radzikowski, J. L., Vedelaar, S., Siegel, D., Ortega, Á. D., Schmidt, A., & Heinemann, M. (2016).
1106 Bacterial persistence is an active σS stress response to metabolic flux limitation. *Molecular*
1107 *Systems Biology*, *12*(9), 882.
1108 Roostalu, J., J\~oers, A., Luidalepp, H., Kaldalu, N., & Tenson, T. (2008). Cell division in
1109 Escherichia coli cultures monitored at single cell resolution. *BMC Microbiology*, *8*, 1–14.
1110 Salgado, H., Peralta-Gil, M., Gama-Castro, S., Santos-Zavaleta, A., Muñiz-Rascado, L., García-
1111 Sotelo, J. S., Weiss, V., Solano-Lira, H., Martínez-Flores, I., Medina-Rivera, A., Salgado-
1112 Osorio, G., Alquicira-Hernández, S., Alquicira-Hernández, K., López-Fuentes, A., Porrón-
1113 Sotelo, L., Huerta, A. M., Bonavides-Martínez, C., Balderas-Martínez, Y. I., Pannier, L., …
1114 Collado-Vides, J. (2013). RegulonDB v8.0: omics data sets, evolutionary conservation,
1115 regulatory phrases, cross-validated gold standards and more. *Nucleic Acids Research*,
1116 *41*(D1), D203–D213. https://doi.org/10.1093/nar/gks1201
1117 Shan, Y., Brown Gandt, A., Rowe, S. E., Deisinger, J. P., Conlon, B. P., & Lewis, K. (2017). ATP-
1118 dependent persister formation in Escherichia coli. *MBio*, *8*(1), 10–1128.
1119 Shan, Y., Lazinski, D., Rowe, S., Camilli, A., & Lewis, K. (2015). Genetic Basis of Persister
1120 Tolerance to Aminoglycosides in Escherichia coli. *MBio*, *6*(2).
1121 https://doi.org/10.1128/mBio.00078-15
1122 Shiraliyev, R. C., & Orman, M. (2023). Metabolic disruption impairs ribosomal protein levels,
1123 resulting in enhanced aminoglycoside tolerance. *BioRxiv*, 2012–2023.
1124 Spoering, A. L., Vulić, M., & Lewis, K. (2006). GlpD and PlsB Participate in Persister Cell
1125 Formation in *Escherichia coli*. *Journal of Bacteriology*, *188*(14), 5136–5144.
1126 https://doi.org/10.1128/JB.00369-06
1127 Sulaiman, J. E., & Lam, H. (2020). Proteomic investigation of tolerant Escherichia coli
1128 populations from cyclic antibiotic treatment. *Journal of Proteome Research*, *19*(2), 900–
1129 913.
1130 Surmann, K., Stopp, M., Wörner, S., Dhople, V. M., Völker, U., Unden, G., & Hammer, E. (2020).
1131 Fumarate dependent protein composition under aerobic and anaerobic growth conditions
1132 in Escherichia coli. *Journal of Proteomics*, *212*, 103583.
1133 https://doi.org/10.1016/j.jprot.2019.103583
1134 Szklarczyk, D., Gable, A. L., Nastou, K. C., Lyon, D., Kirsch, R., Pyysalo, S., Doncheva, N. T.,
1135 Legeay, M., Fang, T., Bork, P., Jensen, L. J., & von Mering, C. (2021). The STRING database
1136 in 2021: customizable protein–protein networks, and functional characterization of user-
1137 uploaded gene/measurement sets. *Nucleic Acids Research*, *49*(D1), D605–D612.
1138 https://doi.org/10.1093/nar/gkaa1074

Szklarczyk, D., Kirsch, R., Koutrouli, M., Nastou, K., Mehryary, F., Hachilif, R., Gable, A. L., Fang, T., Doncheva, N. T., Pyysalo, S., & others. (2023). The STRING database in 2023: protein–protein association networks and functional enrichment analyses for any sequenced genome of interest. *Nucleic Acids Research*, *51*(D1), D638–D646.

Taber, H. W., Mueller, J. P., Miller, P. F., & Arrow, A. S. (1987). Bacterial uptake of aminoglycoside antibiotics. *Microbiological Reviews*, *51*(4), 439–457. https://doi.org/10.1128/mr.51.4.439-457.1987

Tirabassi, R., & Bio, B. (2014). Foundations of Molecular Cloning-Past, Present and Future. *NEB, New England Bio Labs Inc, Www. Neb. Com/Tools-and-Resources/Featurearticles/Foundations-of-Molecular-Cloning-Past-Present-and-Future*.

Tsai, M.-J., Wang, J.-R., Yang, C.-D., Kao, K.-C., Huang, W.-L., Huang, H.-Y., Tseng, C.-P., Huang, H.-D., & Ho, S.-Y. (2018). PredCRP: predicting and analysing the regulatory roles of CRP from its binding sites in Escherichia coli. *Scientific Reports*, *8*(1), 951. https://doi.org/10.1038/s41598-017-18648-5

Vasan, K., Werner, M., & Chandel, N. S. (2020). Mitochondrial metabolism as a target for cancer therapy. *Cell Metabolism*, *32*(3), 341–352.

Vogel, R. F., Entian, K. D., & Mecke, D. (1987). Cloning and sequence of the mdh structural gene of Escherichia coli coding for malate dehydrogenase. *Archives of Microbiology*, *149*(1), 36–42. https://doi.org/10.1007/BF00423133

Vulin, C., Leimer, N., Huemer, M., Ackermann, M., & Zinkernagel, A. S. (2018). Prolonged bacterial lag time results in small colony variants that represent a sub-population of persisters. *Nature Communications*, *9*(1), 4074. https://doi.org/10.1038/s41467-018-06527-0

Wakamoto, Y., Dhar, N., Chait, R., Schneider, K., Signorino-Gelo, F., Leibler, S., & McKinney, J. D. (2013). Dynamic Persistence of Antibiotic-Stressed Mycobacteria. *Science*, *339*(6115), 91–95. https://doi.org/10.1126/science.1229858

Wang, Y., Bojer, M. S., George, S. E., Wang, Z., Jensen, P. R., Wolz, C., & Ingmer, H. (2018). Inactivation of TCA cycle enhances Staphylococcus aureus persister cell formation in stationary phase. *Scientific Reports*, *8*(1), 10849. https://doi.org/10.1038/s41598-018-29123-0

Warburg, O. (1925). The metabolism of carcinoma cells. *The Journal of Cancer Research*, *9*(1), 148–163.

Windels, E. M., Michiels, J. E., Fauvart, M., Wenseleers, T., den Bergh, B., & Michiels, J. (2019). Bacterial persistence promotes the evolution of antibiotic resistance by increasing survival and mutation rates. *The ISME Journal*, *13*(5), 1239–1251.

Yamasaki, R., Song, S., Benedik, M. J., & Wood, T. K. (2020). Persister cells resuscitate using membrane sensors that activate chemotaxis, lower cAMP levels, and revive ribosomes. *Iscience*, *23*(1).

Yu, J., Liu, Y., Yin, H., & Chang, Z. (2019). Regrowth-delay body as a bacterial subcellular structure marking multidrug-tolerant persisters. *Cell Discovery*, *5*(1), 8.

YUEN, K. K. (1974). The two-sample trimmed *t* for unequal population variances. *Biometrika*, *61*(1), 165–170. https://doi.org/10.1093/biomet/61.1.165

1181 Zalis, E. A., Nuxoll, A. S., Manuse, S., Clair, G., Radlinski, L. C., Conlon, B. P., Adkins, J., & Lewis, K.
1182 (2019). Stochastic Variation in Expression of the Tricarboxylic Acid Cycle Produces Persister
1183 Cells. *MBio*, *10*(5). https://doi.org/10.1128/mBio.01930-19
1184 Zaslaver, A., Bren, A., Ronen, M., Itzkovitz, S., Kikoin, I., Shavit, S., Liebermeister, W., Surette, M.
1185 G., & Alon, U. (2006). A comprehensive library of fluorescent transcriptional reporters for
1186 Escherichia coli. *Nature Methods*, *3*(8), 623–628.
1187 Zeng, A., Fan, Y., Di, Z., Wang, Y., & Havlin, S. (2022). *Impactful scientists have higher tendency*
1188 *to involve collaborators in new topics*. https://doi.org/10.1073/pnas
1189 Zeng, J., Hong, Y., Zhao, N., Liu, Q., Zhu, W., Xiao, L., Wang, W., Chen, M., Hong, S., Wu, L., Xue,
1190 Y., Wang, D., Niu, J., Drlica, K., & Zhao, X. (2022). A broadly applicable, stress-mediated
1191 bacterial death pathway regulated by the phosphotransferase system (PTS) and the cAMP-
1192 Crp cascade. *Proceedings of the National Academy of Sciences*, *119*(23).
1193 https://doi.org/10.1073/pnas.2118566119
1194 Zhang, Z., Gosset, G., Barabote, R., Gonzalez, C. S., Cuevas, W. A., & Saier, M. H. (2005).
1195 Functional interactions between the carbon and iron utilization regulators, Crp and Fur, in
1196 Escherichia coli. *Journal of Bacteriology*, *187*(3), 980–990.
1197 https://doi.org/10.1128/JB.187.3.980-990.2005
1198 Zheng, D. (2004). Identification of the CRP regulon using in vitro and in vivo transcriptional
1199 profiling. *Nucleic Acids Research*, *32*(19), 5874–5893. https://doi.org/10.1093/nar/gkh908
1200 Zheng, E. J., Stokes, J. M., & Collins, J. J. (2020). Eradicating Bacterial Persisters with
1201 Combinations of Strongly and Weakly Metabolism-Dependent Antibiotics. *Cell Chemical*
1202 *Biology*. https://doi.org/10.1016/j.chembiol.2020.08.015
1203

1204 **Figure Legends**

1205 **Figure 1: Crp/cAMP Regulation of Persister Cell Formation in the Stationary Phase.** *E. coli* K-12
1206 MG1655 WT and mutant cells at early (t=5 h) and late (t=24 h) stationary phases were
1207 transferred to fresh medium with antibiotics for persister cell quantification. At time points 0, 2,
1208 6, 8, and 20 h, 1 mL of the treated culture was washed with 1X phosphate-buffered saline (PBS)
1209 to remove antibiotics. It was then serially diluted and plated on an agar plate to count the
1210 colony-forming units (CFUs). **(A)** Persister levels of ampicillin-treated culture with an antibiotic
1211 concentration of 200 µg/mL. **(B)** Persister levels of ofloxacin-treated culture with an antibiotic
1212 concentration of 5 µg/mL. **(C)** Persister levels of gentamicin-treated culture with an antibiotic
1213 concentration of 50 µg/mL. The number of biological replicates is n=4 for all panels. Biphasic kill
1214 curves were generated using a non-linear model (see **Materials and Methods**). Statistical
1215 significance tests were conducted using F-statistics (*P<0.05, **P<0.01, ****P<0.0001).
1216 The data for each time point represent the mean value±standard deviation.

1217 **Figure 2: The effect of Crp/cAMP on Persister Cell Metabolism during Stationary Phase. (A)**
1218 MS analysis of *E. coli* K-12 MG1655 WT, Δ*crp*, and Δ*cyaA* at early (t=5 h) and late (t=24 h)
1219 stationary phases. Unsupervised hierarchical clustering was applied to standardized metabolic
1220 data. Each column represents a biological replicate. n=4. **(B)** Pathway enrichment analysis was
1221 conducted using MetaboAnalyst (Lu et al., 2023). Upregulated and downregulated pathways of
1222 the Δ*crp* strain compared to WT in the late stationary growth phase were provided in this
1223 figure. **(C, D)** Pathway enrichment maps comparing metabolites of the TCA cycle, pentose

phosphate metabolism, glycolysis, gluconeogenesis, and pyruvate metabolism in Δ*crp* versus WT for early and late stationary phase conditions, respectively. Circle size corresponds to the ratio of normalized metabolite intensities between mutant and control cells. Blue ($P \leq 0.05$ for dark blue; $0.05 < P < 0.10$ for light blue) and red ($P \leq 0.05$ for dark red; $0.05 < P < 0.10$ for light red) indicate significantly downregulated or upregulated metabolites in the mutant compared to the control. White signifies no significant difference. n=4 for all panels. ESP: Early stationary phase, LSP: Late stationary phase.

Figure 3: Validation of Crp/cAMP-Mediated Metabolic State in Persister Cells Through Proteomics Analysis. Pathway enrichment analysis was conducted in STRING (Szklarczyk et al., 2021, 2023) for upregulated **(panel A)** and downregulated **(panel B)** proteins. Genes highlighted in red are linked with the upregulated protein networks, while genes in blue, gray, and purple correspond to those in the downregulated protein network. The visual network in STRING illustrates protein interactions. In evidence mode, color in the network represents the interaction evidence of data support, derived from curated databases, experimental data, gene neighborhood, gene fusions, co-occurrence, co-expression, protein homology, and text mining (Szklarczyk et al., 2021, 2023).

Figure 4: The Role of Crp/cAMP in Non-Growing Cell Formation. (A, B) Flow cytometry histograms depict mCherry expression in *E. coli* K-12 MG1655 WT, Δ*crp*, and Δ*cyaA* at early (t=5 h) and late (t=24 h) stationary phases, respectively. Cells containing an IPTG-inducible mCherry expression system were cultivated with IPTG. After washing and dilution of early and late stationary phase cells in IPTG-free fresh media, fluorescence was tracked in non-growing and growing cells for 2.5 hours. The panel is a representative biological replicate. Consistent results were seen across all 3 biological replicates. **(C)** Growth curves of WT, Δ*crp*, and Δ*cyaA* cultures were determined using flow cytometry to calculate lag and doubling times. Lag times were calculated using the "Microbial lag phase duration calculator" (Opalek et al., 2022). Doubling times were computed using the formula $t_d = \Delta t/(3.3 \times \mathrm{Log}_{10}(N/N_o))$. n=3. *Statistical significance observed between control and mutant strains ($P < 0.05$, 2-tailed t-test). The data for each time point represent the mean value ± standard deviation.

Figure 5: Crp/cAMP-Mediated Metabolic State of Persister Cells. (A) GFP reporter plasmid introduced into *E. coli* K-12 MG1655 WT, Δ*crp*, and Δ*cyaA* cells to monitor SQR gene activity. Flow cytometry was used to detect activity at early (t=5 h) and late (t=24 h) stationary phases. The panel on the left represents a biological replicate, and the results are consistent across all 3 replicates, as demonstrated in the panel on the right. Statistical significance observed between control and mutant groups (*$P < 0.05$, **$P < 0.01$, ***$P < 0.001$, 2-tailed t-test). **(B)** Redox activities of *E. coli* K-12 MG1655 WT, Δ*crp*, and Δ*cyaA* cells were measured at early (t=5 h) and late (t=24 h) stationary phases by flow cytometry using a RSG dye. This dye fluoresces green after reduction by bacterial reductases. A representative biological replicate is shown (left), with consistent results across all 5 replicates (right). Statistical significance observed between control and mutant groups (*$P < 0.05$, **$P < 0.01$, 2-tailed t-test). **(C)** *E. coli* cells with integrated mCherry expression system used to validate cellular respiration. Cells were diluted into fresh media and treated with ampicillin (200 µg/mL) for 20 hours. Flow cytometry measured the red fluorescence of intact surviving cells. A representative biological replicate is shown, with consistent results across all 3 replicates. **(D)** RSG levels of cells (carrying the mCherry expression

system) at exponential phase (t=3 h); cells before ampicillin treatment; non-lysed (intact) cells after 20 hours of ampicillin treatment; and untreated cells after 20 hours of culturing. A representative biological replicate is shown (left), with consistent results across all 4 replicates (right). Statistical significance observed between intact antibiotic-treated cells and others (*P < 0.05, **P < 0.01, 2-tailed t-test). **(E)** High-throughput screening of mutants from the Keio collection. The mutant strains selected are associated with central metabolism. Stationary phase cells were diluted 100-fold in fresh medium and treated with ampicillin (200 µg/mL) or ofloxacin (5 µg/mL) for 20 hours. Treated cultures were washed, serially diluted, and plated on agar plates to quantify CFUs. **(F)** Genes related to the TCA cycle, ETC, ATP synthase, glycolysis, and pentose phosphate pathway (PPP) were knocked out and then treated with ampicillin (200 µg/mL) or ofloxacin (5 µg/mL) to enumerate CFUs. n=4. Biphasic kill curves were generated using a non-linear model. Statistical significance tests were conducted using F-statistics (*P < 0.05, and **P < 0.01). Each data point represents the mean value ± standard deviation.

Supplementary Figure Legends

Figure 1–figure supplement 1. cAMP concentrations normalized to cell numbers for *E. coli* K-12 MG1655 WT, Δ*crp*, and Δ*cyaA*. The cAMP levels were measured in late stationary phase cultures at 450 nm using the Cyclic AMP XP® Assay Kit (Cell Signaling Technology). n=4. Statistical significance was observed between control and mutant strains (*P < 0.05, ***P < 0.001, One-way ANOVA with Dunnett's multiple comparisons test). The data for each time point represent the mean value ± standard deviation.

Figure 1–figure supplement 2. Genetic perturbation of Crp/cAMP enhanced P_{cyaA} promoter activity, resulting in increased *gfp* expression. Overnight cultures of *E. coli* K-12 MG1655 WT, Δ*crp*, and Δ*cyaA* strains harboring the pMSs201 plasmid, which encodes green fluorescent protein (GFP) under the control of the P_{cyaA} promoter, were diluted 1:1000 into fresh LB medium and incubated at 37°C with shaking at 250 rpm for 24 hours. Cells at the late stationary phase were then collected, diluted in 1X PBS, and analyzed by flow cytometry. n=4. Statistical significance was observed between control and mutant strains (****P < 0.0001, One-way ANOVA with Dunnett's multiple comparisons test). The data for each time point represent the mean value ± standard deviation.

Figure 1–figure supplement 3. Growth curves of *E. coli* K-12 MG1655 WT, Δ*crp*, and Δ*cyaA*. Optical densities of cell cultures at 600 nm (OD_{600}) were measured every hour using a plate reader. n=3. The data for each time point represent the mean value ± standard deviation.

Figure 1–figure supplement 4. Normalized cAMP concentrations of *E. coli* K-12 MG1655 WT. The cAMP concentrations were measured in growth cultures at the indicated time points. First, the cAMP concentrations were normalized to the number of cells. Subsequently, the data were further normalized based on the time point 0 to mitigate errors associated with batch-to-batch assay kit variations and to capture the trend in cAMP levels across the time points. n=8. Statistical significance was observed between time points (**P < 0.01, One-way ANOVA with Dunnett's multiple comparisons test). The data for each time point represent the mean

1308 value ± standard error.

1309 **Figure 1–figure supplement 5. Persister levels of cells carrying the Crp expression system.**
1310 Cells at early (t=5 h) and late (t=24 h) stationary phases were transferred to fresh media with
1311 antibiotics for persister cell quantification. At time points 0, 2, 6, 8, and 20 h, 1 mL of the
1312 treated culture underwent two washes with 1X PBS to remove antibiotics. It was then serially
1313 diluted and plated on an agar plate to count the CFUs. **(A)** Persister levels of ampicillin-treated
1314 culture (200 µg/mL). **(B)** Persister levels of ofloxacin-treated cultures (5 µg/mL). **(C)** Persister
1315 levels of gentamicin-treated culture (50 µg/mL). n=4. Biphasic kill curves were generated using
1316 a non-linear model (see **Materials and Methods**). Statistical significance tests were conducted
1317 using F-statistics (**P < 0.01 and ****P < 0.0001). The data for each time point represent the
1318 mean value ± standard deviation.

1319 **Figure 1–figure supplement 6. Persister levels of *E. coli* K-12 MG1655 WT, Δ*crp*, and Δ*cyaA***
1320 **strains at normalized antibiotic concentrations.** Panels show survival following treatment with
1321 **(A)** ampicillin, **(B)** ofloxacin, and **(C)** gentamicin. After treatment, samples were washed six
1322 times with 1X PBS to minimize antibiotic carryover. Antibiotic concentrations were normalized
1323 to MICs to ensure valid comparisons across strains (The concentrations of 33× MIC for
1324 ampicillin and 100× MIC for ofloxacin and gentamicin match those used in Figure 1). n=4.
1325 Statistical significance was observed between control and mutant strains (****P < 0.0001, One-
1326 way ANOVA with Dunnett's multiple comparisons test). The data for each time point represent
1327 the mean value ± standard deviation.

1328 **Figure 1–figure supplement 7. Agar plates showing *E. coli* K-12 MG1655 WT, Δ*crp*, and Δ*cyaA***
1329 **strains following treatment with antibiotics at normalized concentrations.** After treatment,
1330 cells were washed and subjected to 10-fold serial dilutions, then plated on agar. Plates were
1331 incubated for **(A)** 16 h, **(B)** 48 h, and **(C)** 72 h to assess colony formation over time. The panel
1332 is a representative biological replicate. Consistent results were seen across all 3 biological
1333 replicates.

1334 **Figure 1–figure supplement 8. Deletion of *crp* and *cyaA* reduces ampicillin and ofloxacin**
1335 **persistence in the *hipA7* strain.** Persistence levels were assessed by exposing *E. coli* K-12
1336 MG1655 WT, *hipA7*, *hipA7Δcrp*, and *hipA7ΔcyaA* strains in the late stationary phase to the
1337 specified antibiotics, followed by CFU quantification at designated time points. **(A)** Ampicillin
1338 (200 µg/ml), **(B)** Ofloxacin (5 µg/ml) and **(C)** Gentamicin (50 µg/ml). n=4. Statistical significance
1339 was observed between control and mutant strains (****P < 0.0001, One-way ANOVA with
1340 Dunnett's multiple comparisons test). The data for each time point represent the mean
1341 value ± standard deviation.

1342 **Figure 2–figure supplement 1. The pathway enrichment analysis comparing WT and Δ*crp***
1343 **strains during the early stationary phase cultures.** The analysis was conducted using
1344 MetaboAnalyst, with a threshold ratio (Δ*crp*/WT) set at ≤ 0.5 for downregulation and ≥ 2 for
1345 upregulation. **(A)** Upregulated and **(B)** Downregulated pathways in the Δ*crp* strain compared to
1346 WT during the early stationary growth phase (ESP).

1347 **Figure 2–figure supplement 2. The pathway enrichment analysis for the WT strain.** The
1348 analysis was conducted using MetaboAnalyst, with a threshold ratio (LSP/ESP) set at ≤ 0.5 for

1349 downregulation and ≥ 2 for upregulation. **(A)** Upregulated and **(B)** Downregulated pathways of
1350 the WT strain in the late stationary growth phase (LSP) compared to the WT strain in the early
1351 stationary phase (ESP).

1352 **Figure 2–figure supplement 3. The pathway enrichment analysis for the Δ*crp* strain.** The
1353 analysis was conducted using MetaboAnalyst, with a threshold ratio (LSP/ESP) set at ≤ 0.5 for
1354 downregulation and ≥ 2 for upregulation. **(A)** Upregulated and **(B)** Downregulated pathways of
1355 the Δ*crp* strain in the late stationary growth phase (LSP) compared to the Δ*crp* strain in the
1356 early stationary phase (ESP).

1357 **Figure 3–figure supplement 1. The MS analysis of proteins from both WT and Δ*crp* strains at**
1358 **the late stationary phase.** The proteomic data were subjected to unsupervised hierarchical
1359 clustering. Each column in the figure represents a biological replica. n=3.

1360 **Figure 4–figure supplement 1. Persister levels of *E. coli* WT, Δ*crp*, and Δ*cyaA* cells with the**
1361 **integrated mCherry expression system.** Late stationary phase cultures (t=24 h) were
1362 transferred to fresh media and treated with ampicillin (200 µg/mL), ofloxacin (5 µg/mL), and
1363 gentamicin (50 µg/mL) for 20 hours. Subsequently, 1 mL of the treated culture underwent two
1364 washes with 1X PBS to remove antibiotics. It was then serially diluted and plated on an agar
1365 plate to count the CFUs. The levels of ofloxacin and gentamicin persisters in the mutant strains
1366 were below the limit of detection. n=4. Statistical significance was observed between control
1367 and mutant strains (***P < 0.001, ****P < 0.0001, Two-way ANOVA with Tukey's multiple
1368 comparisons test). The data for each time point represent the mean value ± standard
1369 deviation.

1370 **Figure 4–figure supplement 2. Non-growing cell levels in the *E. coli* strain carrying the Crp**
1371 **expression system. (A, B)** Flow cytometry histograms depict mCherry expression in
1372 Δ*crp*+pUA66-*crp*, and Δ*crp*+pUA66 EV at early (t=5 h) and late (t=24 h) stationary phases,
1373 respectively. Cells containing an IPTG-inducible mCherry expression system were cultivated
1374 with IPTG. After washing and dilution of early and late stationary phase cells in IPTG-free fresh
1375 media, fluorescence was tracked in non-growing and growing cells for 2.5 hours. The panel is a
1376 representative biological replicate. Consistent results were seen across all 3 biological
1377 replicates.

1378 **Figure 5–figure supplement 1. RSG staining control for bacterial metabolic activities.**
1379 Exponential phase (t=3 h) cells were stained with 1 µM RSG for 10 minutes at 37°C before
1380 analyzing by flow cytometry. Unstained cells and cells treated with 20 µM CCCP + 1 µM RSG
1381 were used as control. CCCP was expected to reduce cellular redox activities. The panel is a
1382 representative biological replicate. Consistent results were seen across all 3 biological
1383 replicates.

1384 **Figure 5–figure supplement 2. Intact (non-lysed) cell levels of *E. coli* WT, Δ*crp*, and Δ*cyaA* cells**
1385 **with the integrated mCherry expression system.** mCherry positive cells were diluted into fresh
1386 media and treated with ampicillin (200 µg/mL) for 20 hours. Flow cytometry was used to
1387 measure the red fluorescence of intact surviving cells at time points t=0, 1, 2, 4, 6 and 20 h. A
1388 representative biological replicate is shown, with consistent results across all 3 replicates.

1389 **Figure 5–figure supplement 3. VBNC levels of *E. coli* WT, Δ*crp*, and Δ*cyaA* cells with the**

integrated mCherry expression system. Flow cytometry was employed to quantify intact surviving cells. Persister cells were quantified by plating the cells on agar media. Viable but nonculturable (VBNC) cells were enumerated by subtracting persister levels from the intact cell levels. n=4. Statistical significance was observed between control and mutant strains (****P < 0.0001, One-way ANOVA using Dunnett's multiple comparisons test). The data for each time point represent the mean value ± standard deviation.

Figure 5–figure supplement 4. Cell counts of *E. coli* K-12 MG1655 WT and mutant strains using flow cytometry at late stationary phase. Cells were diluted 100-fold into 1 mL of 1X PBS. n=4. The data for each time point represent the mean value ± standard deviation.

List of Supplementary Files

Supplementary File 1. MIC of antibiotics and concentrations of bactericidal antibiotics used in persister assays.
Supplementary File 2. Analyzed metabolomics data.
Supplementary File 3. Analyzed proteomics data.
Supplementary File 4. Analyzed persister survival fraction data.
Supplemental File 5. The knockout strains generated using the *E. coli* K-12 MG1655 background in this study.
Supplemental File 6. Persister levels of *E. coli* K-12 MG1655 WT, Δ*crp*, and Δ*cyaA* strains in late stationary phase.
Supplemental File 7. Persister levels of *E. coli* K-12 MG1655 (A) and BW25113 (B) WT, Δ*crp*, and Δ*cyaA* strains in the exponential growth phase.

List of Source Data

Figure 2 - Source Data 1: Normalized Metabolomics Data of Early and Late Stationary Phases of Wild-Type and Mutant *crp* Across 3 Biological Replicates. Data Collected and Analyzed by Metabolon Inc. (Morrisville, NC).
Figure 3 - Source Data 1: Normalized Proteomics Data of the Late Stationary Phase of Wild-Type and Mutant *crp* Across 3 Biological Replicates. Data Collected by UT Health's Clinical and Translational Proteomics Service Center (Houston, TX).

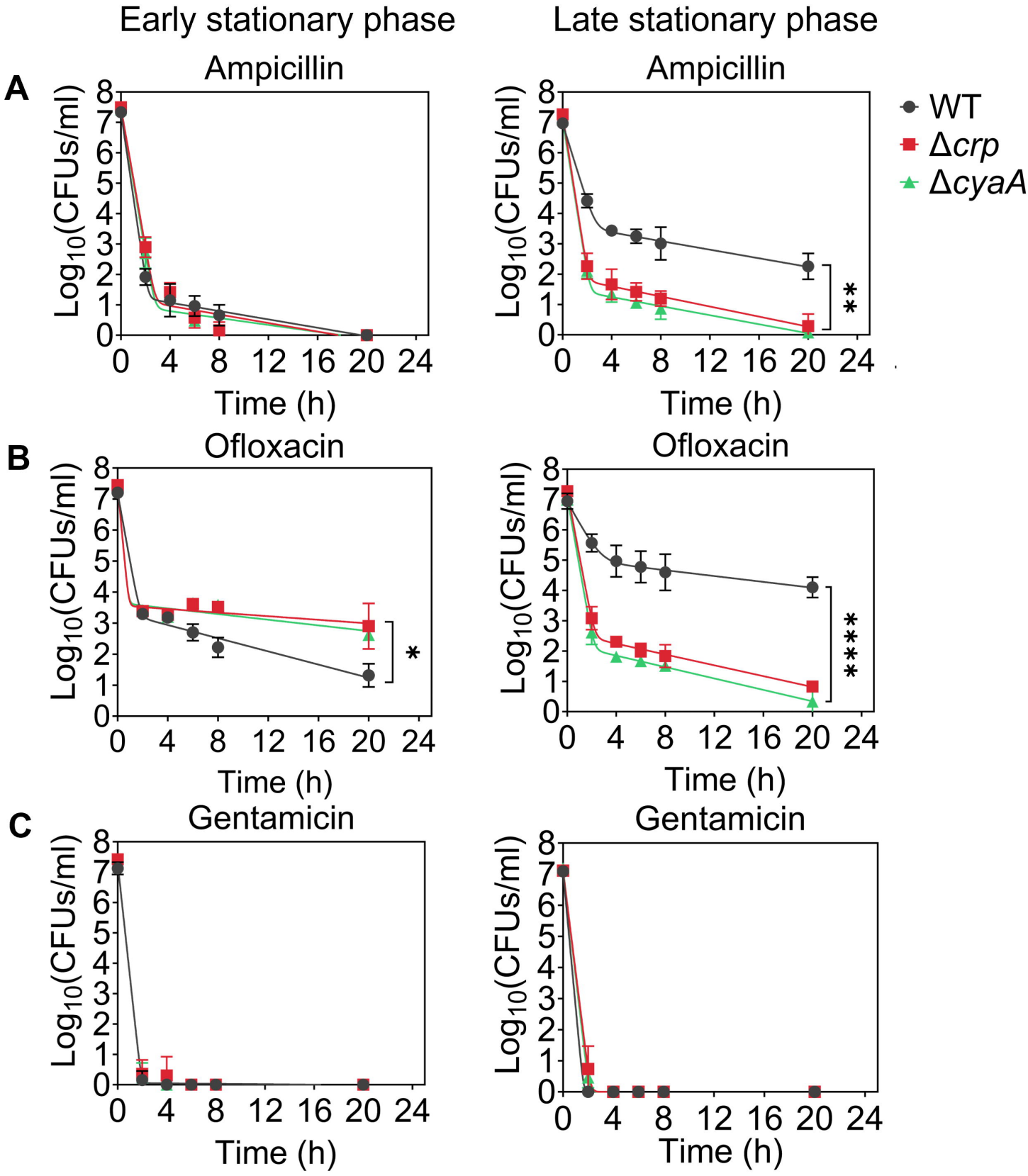
Early stationary phase
Late stationary phase
A
Ampicillin
Ampicillin
B
Ofloxacin
Ofloxacin
C
Gentamicin
Gentamicin
Log10(CFUs/ml)
Time (h)
WT
Δcrp
ΔcyaA
**
*
****

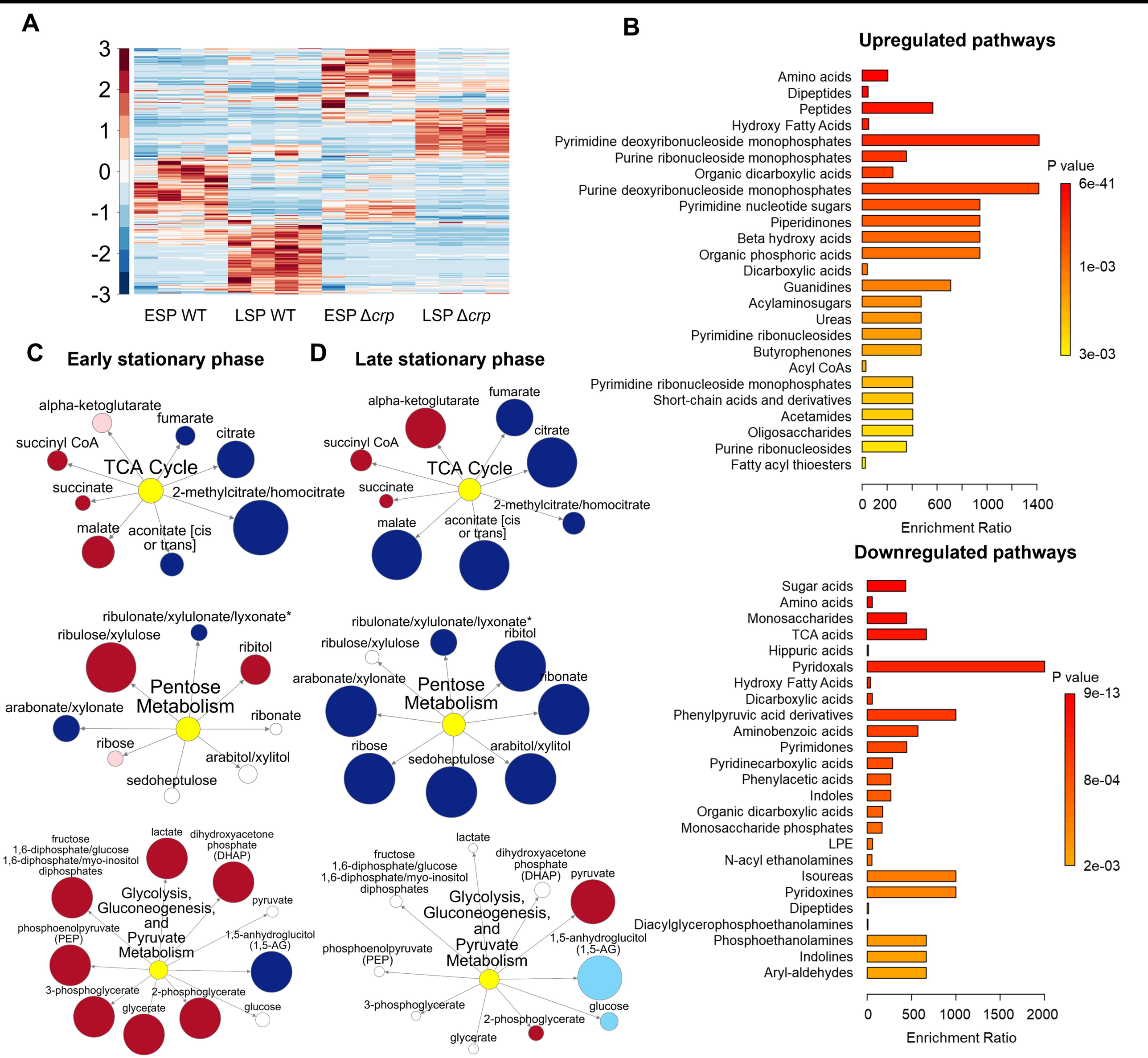

Upregulated (red circle) and downregulated (blue circle) metabolites in the Δ*crp* strain compared to WT

A Upregulated pathways

- Anabolic metabolism
- Peptidoglycan metabolic processes
- Cell wall organization or biogenesis
- Cellular component organization or biogenesis
- Regulation of cell shape, cell cycle, and cell division

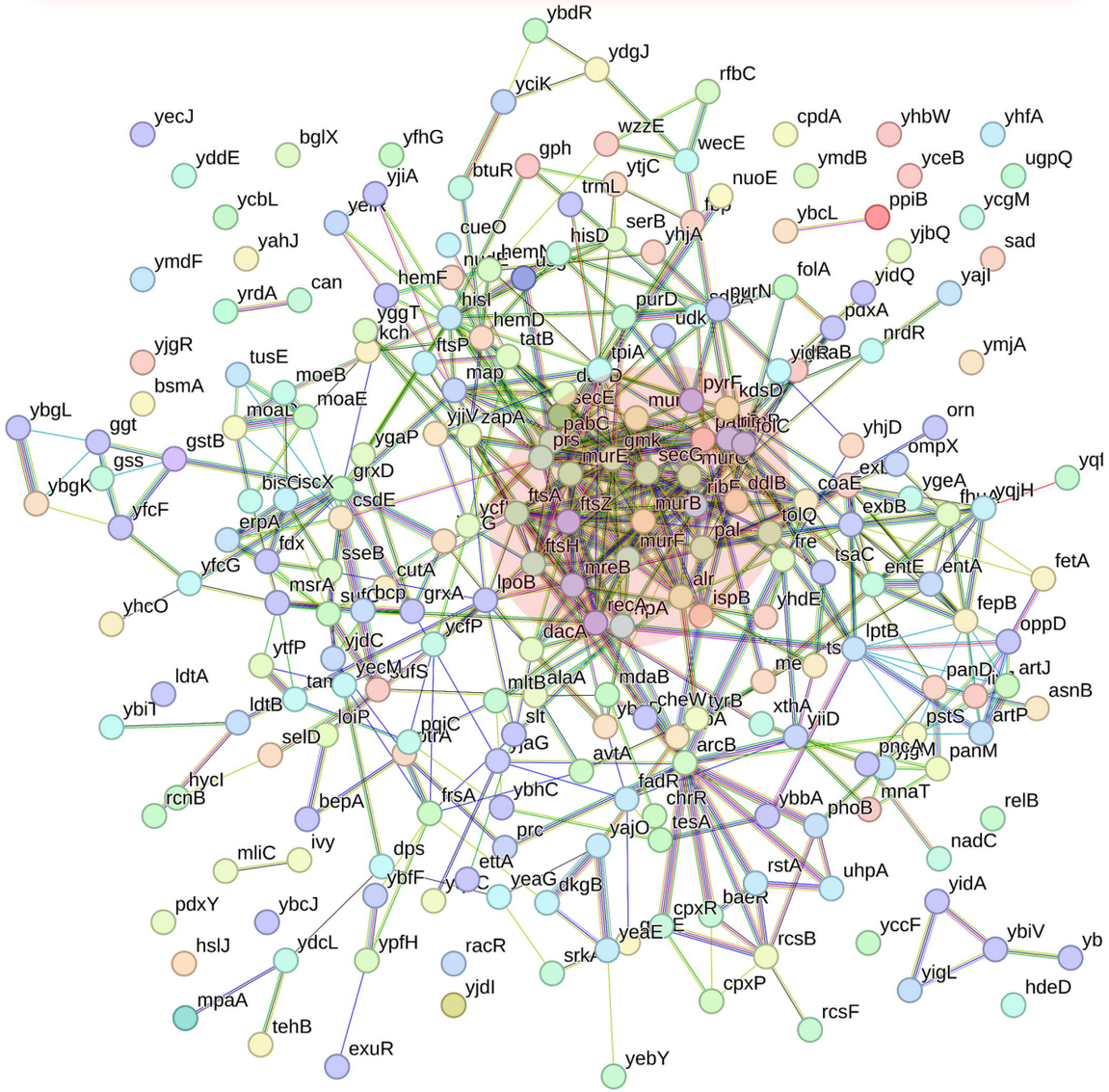

B Downregulated pathways

- Ribosome and translation factor activity
- Translation, and protein export
- Ribonucleoprotein, and translation factor activity
- RNA binding

- Tricarboxylic acid cycle
- Glycerol metabolism
- Pyruvate metabolism
- Glycolysis
- Energy metabolism
- Respiratory processes

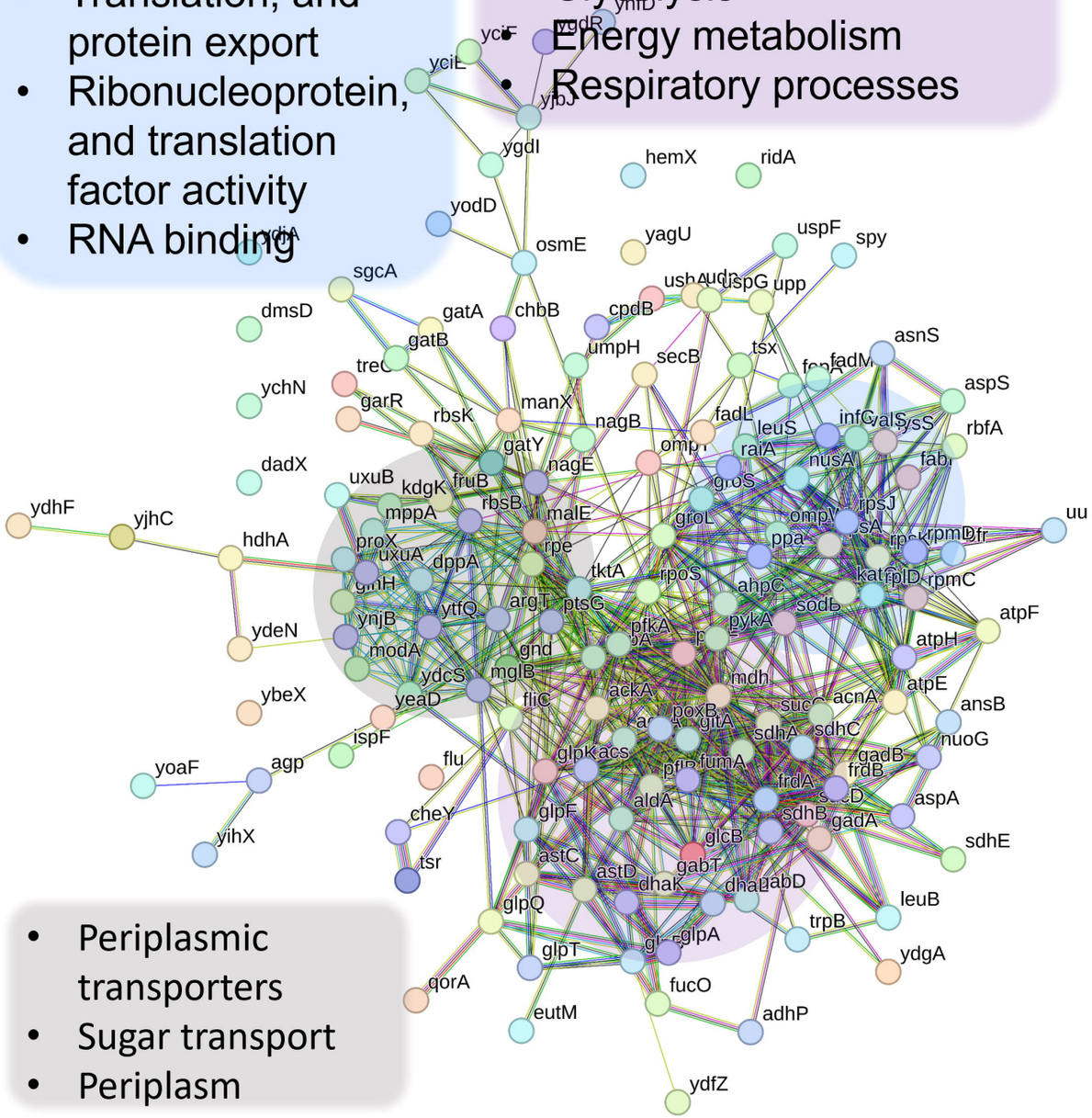

- Periplasmic transporters
- Sugar transport
- Periplasm

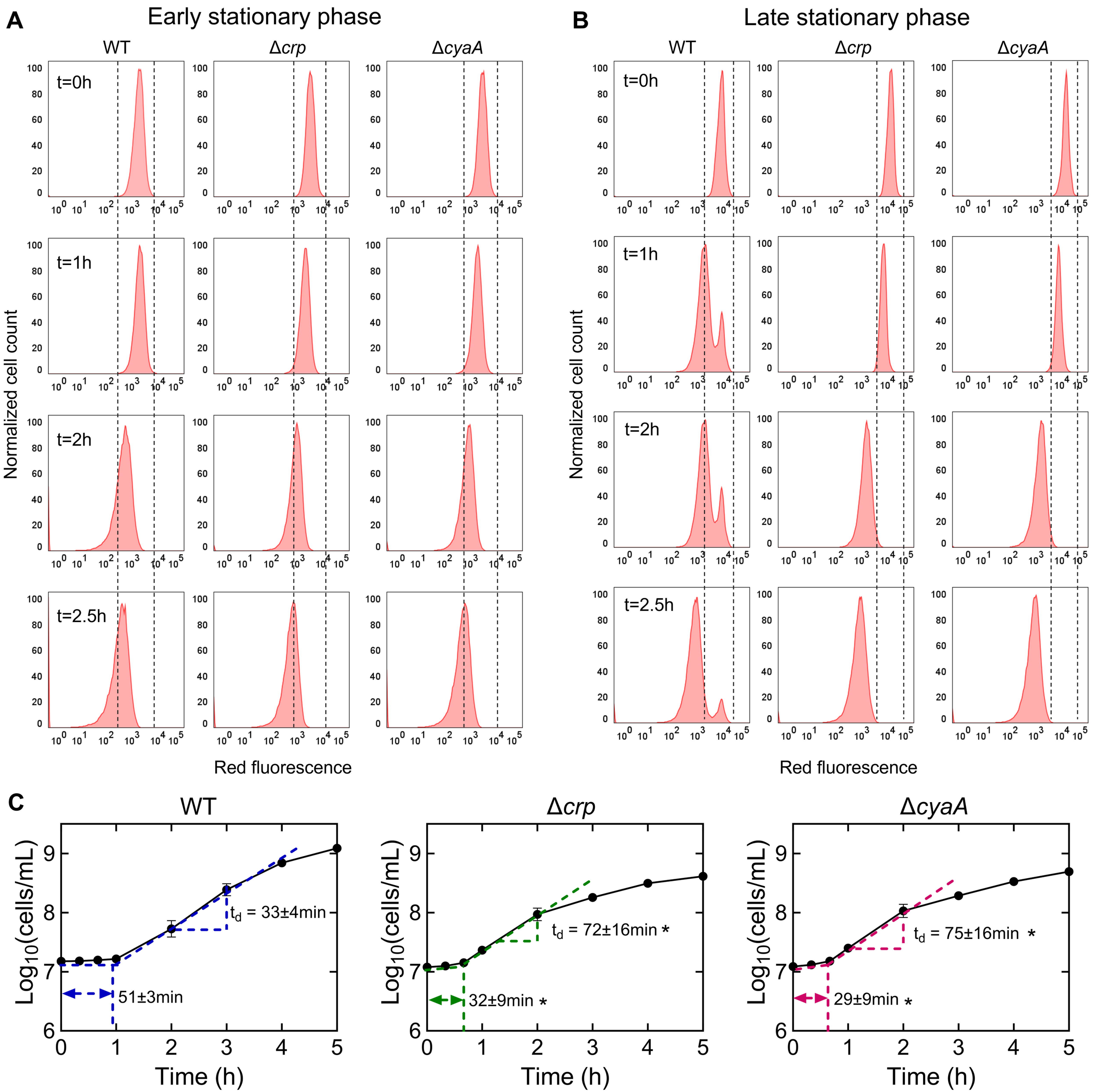
A
Early stationary phase
WT
Δcrp
ΔcyaA
t=0h
t=1h
t=2h
t=2.5h
Normalized cell count
Red fluorescence
B
Late stationary phase
WT
Δcrp
ΔcyaA
t=0h
t=1h
t=2h
t=2.5h
Normalized cell count
Red fluorescence
C
WT
Δcrp
ΔcyaA
Log10(cells/mL)
Time (h)
td = 33±4min
51±3min
td = 72±16min *
32±9min *
td = 75±16min *
29±9min *

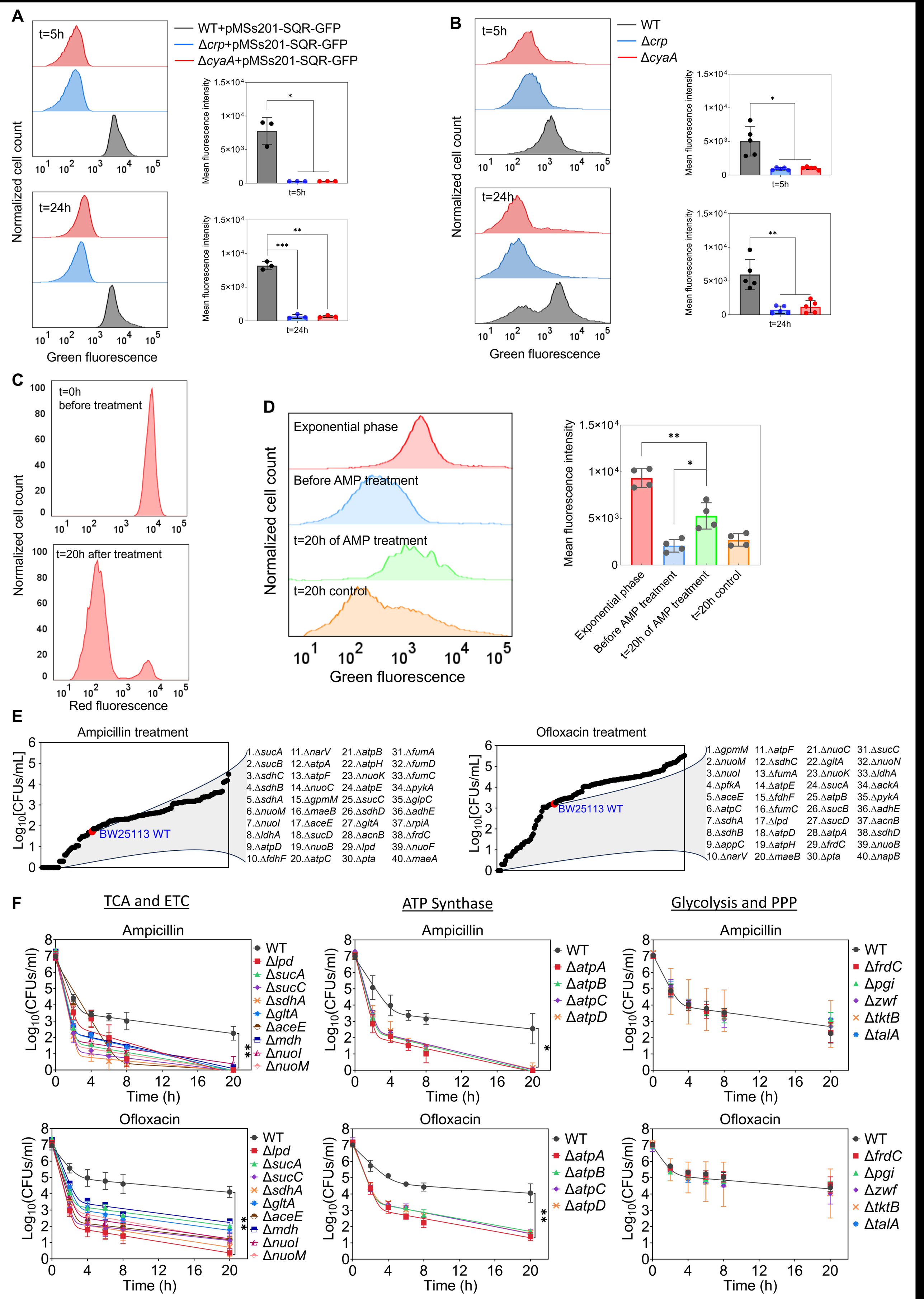
A
t=5h
t=24h
WT+pMSs201-SQR-GFP
Δcrp+pMSs201-SQR-GFP
ΔcyaA+pMSs201-SQR-GFP
Normalized cell count
Green fluorescence
Mean fluorescence intensity
B
WT
Δcrp
ΔcyaA
C
t=0h
before treatment
t=20h after treatment
Red fluorescence
D
Exponential phase
Before AMP treatment
t=20h of AMP treatment
t=20h control
E
Ampicillin treatment
Ofloxacin treatment
Log10[CFUs/mL]
BW25113 WT
1.ΔsucA 2.ΔsucB 3.ΔsdhC 4.ΔsdhB 5.ΔsdhA 6.ΔnuoM 7.ΔnuoI 8.ΔldhA 9.ΔatpD 10.ΔfdhF 11.ΔnarV 12.ΔatpA 13.ΔatpF 14.ΔnuoC 15.ΔgpmM 16.ΔmaeB 17.ΔaceE 18.ΔsucD 19.ΔnuoB 20.ΔatpC 21.ΔatpB 22.ΔatpH 23.ΔnuoK 24.ΔatpE 25.ΔsucC 26.ΔsdhD 27.ΔgltA 28.ΔacnB 29.Δlpd 30.Δpta 31.ΔfumA 32.ΔfumD 33.ΔfumC 34.ΔpykA 35.ΔglpC 36.ΔadhE 37.ΔrpiA 38.ΔfrdC 39.ΔnuoF 40.ΔmaeA
1.ΔgpmM 2.ΔnuoM 3.ΔnuoI 4.ΔpfkA 5.ΔaceE 6.ΔatpC 7.ΔsdhA 8.ΔsdhB 9.ΔappC 10.ΔnarV 11.ΔatpF 12.ΔsdhC 13.ΔfumA 14.ΔatpE 15.ΔfdhF 16.ΔfumC 17.Δlpd 18.ΔatpD 19.ΔatpH 20.ΔmaeB 21.ΔnuoC 22.ΔgltA 23.ΔnuoK 24.ΔsucA 25.ΔatpB 26.ΔsucB 27.ΔsucD 28.ΔatpA 29.ΔfrdC 30.Δpta 31.ΔsucC 32.ΔnuoN 33.ΔldhA 34.ΔackA 35.ΔpykA 36.ΔadhE 37.ΔacnB 38.ΔsdhD 39.ΔnuoB 40.ΔnapB
F
TCA and ETC
ATP Synthase
Glycolysis and PPP
Ampicillin
Ofloxacin
Log10(CFUs/ml)
Time (h)
WT
Δlpd
ΔsucA
ΔsucC
ΔsdhA
ΔgltA
ΔaceE
Δmdh
ΔnuoI
ΔnuoM
ΔatpA
ΔatpB
ΔatpC
ΔatpD
ΔfrdC
Δpgi
Δzwf
ΔtktB
ΔtalA